INFLUENCE OF PARTICLE SHAPE AND BED HEIGHT ON FLUIDIZATION

By

LINGZHI LIAO

A THESIS PRESENTED TO THE GRADUATE SCHOOL
OF THE UNIVERSITY OF FLORIDA IN PARTIAL FULFILLMENT
OF THE REQUIREMENTS FOR THE DEGREE OF
MASTER OF SCIENCE

UNIVERSITY OF FLORIDA

2013

To my mom and dad

ACKNOWLEDGMENTS

I would like to express my gratitude to my advisor Prof. Jennifer S. Curtis for teaching me how to be a researcher, guiding me with patience, and encouraging me all the time. I am also grateful to my dear parents for supporting me, loving me, and trusting in me unconditionally. I would also like to acknowledge my committee member Dr. Kevin Powers for his instruction and suggestions. Additionally, my thanks go to my colleagues, Yu Guo, Casey LaMarche, Sarah Mena, Poom Buncha, Deepak Rangrajan, and Henna Tangri, for offering to help with my research and for sharing their experience; to my friends, Jie Han, Dan Mao, Yang Song, and Linli Hu, for taking care of me and backing me up; and to Jim Hinnant, Dennis L. Vince, Shirley A. Kelly, Deborah D. Sandoval, Carolyn Miller, and all the officers who helped me.

My special thanks are extended to Santiago A. Tavares, Claire Eder, and Dr. Seymour S. Block for their generous help in improving my thesis.

TABLE OF CONTENTS

page

LIST OF TABLES

LIST OF FIGURES

NOMENCLATURE

A	Cross area of fluidized bed, cm^2
A_p	Surface area of particles, μm^2
Ar	Archimedes number, dimensionless
D_{in}	Inner diameter of cylinder test vessel, cm
D_p	Particle diameter, μm
D_v	Equivalent volume diameter, μm
g	Gravitational acceleration, m/s^2
g_c	Standard gravitational acceleration, 9.806 m/s^2
$H_{initial}$	Initial height of fluidized bed, cm
H_{mf}	Height of fluidized bed at minimum fluidization, cm
m_p	Mass of particles, g
$(-\Delta P)$	Pressure drop, mm in water
Re	Reynolds number, dimensionless
Re_{mf}	Reynolds number at minimum fluidization, dimensionless
U_{mf}	Minimum fluidization velocity, m/s
V_p	Volume of particles, μm^3

Greeks

ε	Voidage of fluidized bed, dimensionless
ε_m	Voidage of fluidized bed at minimum fluidization, dimensionless
ρ_f	Density of fluid, g/cm^3
ρ_p	Density of particles, g/cm^3
Φ	Sphericity of particles, dimensionless
μ	Viscosity of fluid, kg/m/s

Abstract of Thesis Presented to the Graduate School
of the University of Florida in Partial Fulfillment of the
Requirements for the Degree of Master of Science

INFLUENCE OF PARTICLE SHAPE AND BED HEIGHT ON FLUIDIZATION

By

Lingzhi Liao

May 2013

Chair: Jennifer S. Curtis
Major: Chemical Engineering

Fluidized beds have been widely used in industry. The minimum fluidization velocity is not only a crucial factor for reaction design; it is also an important index for process control. Compared to other parameters, the effects of bed voidage and particle sphericity on minimum fluidization velocity are obscure and difficult to predict. Therefore, the present work investigates the fluidization behavior of particles with different sphericity. It is found that as the sphericity decreases, the bed voidage increases. Increasing the particle density and initial bed height causes the voidage to decrease due to the strong compression in the bed. The decrease in the voidage can lead to a decrease in the minimum fluidization velocity.

Channeling appears in the fluidization process of flakes that have a sphericity of less than 0.6, even when the flakes are characterized as Group B particles. Additionally, channeling becomes more significant as the sphericity decreases. This cohesive fluidization behavior of flakes can be better described by the redefining the particle diameter D_p as the ratio of volume to surface area. In addition, a modification of the boundary between Geldart's Groups A and C is proposed.

CHAPTER 1
INTRODUCTION

Over the last century, fluidized beds have been rapidly developed and popularized in industry. For coal combustion, mineral, and metallurgical processes, fluidized bed combustions stand out due to its capability of operating at a continuous stage, providing homogeneous thermal distribution not only inside the fluidized bed but also between materials and their container, and enhancing contact opportunities between solid and fluid materials. For coal gasification, nuclear power plants, water and waste treatment, and other chemical reactions, fluidized beds bring advantages such as their uniform mixture of materials, and large contact area, which lead to effective and efficient chemical reactions and heat transfer. The catalytic cracking process is another of the earliest applications of fluidized bed.

However, there are some uncertain factors that have hindered the design, optimization, and scale up of fluidized beds. One of the uncertain factors is the operation temperature for a gas-solid system. Studies have shown that in addition to its influence on gas properties, temperature could also affect voidage at minimum fluidization, the minimum fluidization velocity, and the minimum bubbling velocity [1]. To eliminate the influence of temperature on gas properties, Wen-Ching Yang [2] proposed using Archimedes number to replace particle diameter while using dimensionless density to replace particle density, which is defined as the ratio of the difference between particle density and fluid density to the fluid density. Wall effect is another controversial element: it exerts a direct influence on the pressure drop of fluidized beds. The ratio of the test vessel diameter to the particle diameter is the main variable used to indicate the severity of the wall effect. Moreover, the influence of wall effect on pressure

drop varies at different flow regimes [3, 4]. The influence of wall effect also varies based on a difference in particle shape [4]. The way size distribution affects fluidization is unknown, as well. In industries, particles are seldom monodisperse; additionally, the size distribution of particles varies from one type to another. D. Gauthier etc. [5] and C. Lin etc. [6] studied four classifications of mixtures at room temperature and high temperature respectively. The four classifications of mixtures were a binary mixture, a uniform distribution, a narrow cut, and a Gaussian distribution. It was concluded that the mean diameter of particles was insufficient to represent polydisperse particles, and that different mixtures could lead to different behaviors in fluidized beds. Large size distribution may also result in the particles' entrainment in fluidized beds. Moreover, other factors, such as inter-particle forces, the fluidized bed's shape and size, and the materials used in the fluidized bed, can also influence fluidization to a certain extent. However, those effects have only been qualitatively generalized; the research failed to produce a clear and quantitative description. Thus, a rigorous and accurate prediction is not available for fluidized beds.

CHAPTER 2
BACKGROUND

A packed bed is a column filled with packing materials. Liquid or gas can flow through a packed bed to achieve separation or reactions. For sufficiently low flow rates, the fluid passes through the void space between particles without disturbing them. This case is referred to as a “fixed bed.” At higher flow rates, the drag forces generated by the pressure difference acting on the particles can exceed the gravitational force and lift up the particles. However, when the bed of particles expands, the drag force drops because of a reduction in the fluid velocity in the void spaces. This results is a highly dynamic state that we refer to as fluidization.

When fluidizing solid particles in a packed bed, there is a pressure drop across the unit that causes energy losses. Several researchers have expressed concerns about the relationship between the energy losses and the properties of fluids and solids, and equations describing this relationship have been derived based on theoretical analysis and experimental data. The most widely accepted equations are the Carman-Kozeny equation, the Burke-Plummer equation, and the Ergun equation. [7]

It is commonly believed that for a laminar flow, with low Reynolds numbers—that is, up to 10, where the viscous-energy losses dominate—the Carman-Kozeny equation is valid, as shown below (Eq. 2-1)

$$\frac{(-\Delta P)}{H} = 180\,\frac{\mu U}{g_c \Phi^2 D_v^2}\,\frac{(1-\varepsilon)^2}{\varepsilon^3} \qquad (2\text{-}1)$$

where (-ΔP) is the frictional pressure drop across a bed depth H, U is the superficial fluid velocity, μ is the viscosity of fluid, Φ and D_v are the sphericity and the equivalent volume diameter of packing materials, ε is the voidage of the packed bed, and g_c is the

standard gravitational acceleration. In addition, the diameter of non-spherical particles is assumed to be described as the equivalent volume diameter times the sphericity of particles.

As the fluid velocity increases, the flow is no longer a laminar flow and becomes turbulent with higher Reynolds numbers (Greater than 2000). The kinetic-energy losses caused by changing channel cross-section and fluid flow direction are the main contributor to the pressure drop. In this case, the Burke-Plummer equation, as shown below (Eq. 2-2), has to be taken into consideration.

$$\frac{(-\Delta P)}{H} = 1.75 \frac{\rho_f U^2}{g_c \Phi D_v} \frac{(1-\varepsilon)}{\varepsilon^3} \qquad (2\text{-}2)$$

where ρ_f is the density of fluid.

Assuming that the viscous losses and the kinetic energy losses are additive and simultaneous, the pressure drop in entire region from laminar to turbulent, can be obtained using the Ergun equation, as shown below (Eq. 2-3), which is the summation of Eq.2-1 and 2-2.

$$\frac{(-\Delta P)}{H} = 150 \frac{\mu U}{g_c \Phi^2 D_v^2} \frac{(1-\varepsilon)^2}{\varepsilon^3} + 1.75 \frac{\rho_f U^2}{g_c \Phi D_v} \frac{(1-\varepsilon)}{\varepsilon^3} \qquad (2\text{-}3)$$

Minimum Fluidization Velocity

With the increase in fluid velocity, the drag force can become sufficient to balance the gravity of the solids. This dynamic equilibrium occurs at a minimum fluidization velocity and is known as incipient fluidization. Once this minimum fluidization velocity is reached, the fluidized bed is formed.

When fluidization is about to occur, the pressure drop no longer depends on the fluid velocity and stays constant at a certain range, which can be expressed as follows (Eq. 2-4).

$$-\Delta P = \frac{g}{g_c}(1-\varepsilon_m)(\rho_p - \rho_f)H \tag{2-4}$$

where ε_m is the voidage of packed bed at minimum fluidization, and ρ_p is the density of particles.

The substitution of Eq. 2-4 into the Ergun equation (Eq. 2-3) gives Eq. 2-5 shown below, which lead to a quadratic equation for the minimum fluidization velocity (U_{mf}).

$$g(\rho_p - \rho_f) = 150\frac{\mu U_{mf}}{\Phi^2 D_v^2}\frac{(1-\varepsilon_m)}{{\varepsilon_m}^3} + 1.75\frac{\rho_f U_{mf}^2}{\Phi D_v}\frac{1}{{\varepsilon_m}^3} \tag{2-5}$$

In order to simplify the form of the Ergun equation at incipient fluidization, two dimensionless numbers (Archimedes Number (Ar) and Reynolds Number (Re)) have been introduced.

The Archimedes Number (Ar) is the ratio of the gravitational forces to the viscous forces, as shown in Eq. 2-6.

$$Ar = \frac{D_v^3 \rho_f (\rho_p - \rho_f) g}{\mu^2} \tag{2-6}$$

The Reynolds Number (Re_{mf}) which is defined as the ratio of inertial forces to viscous forces at incipient fluidization, as shown in Eq. 2-7.

$$Re_{mf} = \frac{D_v U_{mf} \rho_f}{\mu} \tag{2-7}$$

When substituting Ar (Eq. 2-6) and Re_{mf} (Eq. 2-7) into the Ergun Equation at incipient fluidization (Eq. 2-5), Eq. 2-8, shown below, is obtained.

$$Ar = 150\frac{(1-\varepsilon_m)}{\Phi^2{\varepsilon_m}^3}Re_{mf} + 1.75\frac{1}{\Phi{\varepsilon_m}^3}Re_{mf}^2 \quad (2\text{-}8)$$

When solving for the minimum fluidization velocity using Eq. 2-8, a problem that arised when trying to get values for the sphericity Φ and voidage at minimum fluidization ε_m.

Key Parameters That Affect Minimum Fluidization Velocity

Diameter of Particle

Equivalent volume diameter is defined as the diameter of a sphere that has the same volume as the particle. Surface to volume diameter is defined as the diameter of a sphere that has the same surface area to volume ratio as the particle.

Sphericity of Particle

Sphericity is an important measure that describes how round a particle is. It is defined as the ratio of the surface area of a sphere with the same volume as the given particle to the surface area of the particle itself, as described in Eq. 2-9.

$$\Phi = \frac{\pi^{\frac{1}{3}}(6V_p)^{\frac{2}{3}}}{A_p} \quad (2\text{-}9)$$

A sphere has sphericity of 1. Some regular shape particles have a fixed value of sphericity, as shown in Figure 2-1 [8] . However, most particles do not have a regular shape and their sphericity is affected by other parameters, such as aspect ratio.

Voidage at Minimum Fluidization

Voidage is defined as the ratio of the volume of interspace between particles to the volume of packed bed, as shown in Eq. 2-10. Voidage at minimum fluidization has the same definition, except both volumes are obtained at incipient fluidization.

$$\varepsilon = \frac{Volume\ of\ the\ voids}{Overall\ Volume} \quad (2\text{-}10)$$

Fluid Properties

The viscosity and density of the fluid exert influence on the minimum fluidization velocity, as well. In the case of air, its viscosity and density are dependent on the environmental temperature and humidity.

Correlations from the Literature Used to Predict Minimum Fluidization Velocity

Researchers have devised solutions to the problem of finding Φ and ε_m. Some of these adaptions include simplifications to the Ergun equation, modifications to the Carman-Kozeny equation and the combination of dimensionless terms. A brief description for these three approaches follows.

Simplification of the Ergun Equation

The first form of prediction correlation is based on the Ergun equation at incipient fluidization. Researchers replaced the coefficients $\frac{(1-\varepsilon_m)}{\Phi^2 {\varepsilon_m}^3}$ and $\frac{1}{\Phi \varepsilon_m{}^3}$ on the Ergun equation with two constants based on fitting the literature data to proposed equations. In other words, this method simplifies Eq. 1-8 into Eq. 2-11 as shown below:

$$Ar = C_1 \cdot Re_{mf} + C_2 \cdot Re_{mf}^2 \qquad (2\text{-}11)$$

where C_1 and C_2 are constants.

U_{mf} can now be obtained simply by solving quadratic equation 2-11. The most famous correlation solving C_1 and C_2 is Wen & Yu's equation [9], as shown below (Eq. 2-12).

$$Re_{mf} = [(33.7)^2 + 0.0408Ar]^{0.5} - 33.7 \qquad (2\text{-}12)$$

However, this form of predictive correlation entailed relatively large error of 30-40%, and is only valid for limited conditions. Besides, the assumed relationships

$\frac{(1-\varepsilon_m)}{\Phi^2 {\varepsilon_m}^3} = C_1$ and $\frac{1}{\Phi {\varepsilon_m}^3} = C_2$ are not valid for all Φ and ε_m. Other scientists used the same method and found different values for the constants. A summary of their findings is shown in Table 2-1.

Modification of the Carman-Kozeny Equation

The second option is a modification of the Carman-Kozeny equation at incipient fluidization. As shown below, Eq. 2-13 is the original form of the Carman-Kozeny equation at incipient fluidization.

$$Ar = 180 \frac{(1-\varepsilon_m)}{\Phi^2 {\varepsilon_m}^3} Re_{mf} \qquad (2\text{-}13)$$

As before, Researchers [10, 11] made the same assumption that was shown in the first method—they replaced the coefficient $\frac{(1-\varepsilon_m)}{\Phi^2 {\varepsilon_m}^3}$ with a constant. Additionally, they changed the linear relationship between Ar and Re_{mf} into an exponential relationship. The general form of this method is shown in Eq. 2-14.

$$Re_{mf} = a \cdot Ar^b \qquad (2\text{-}14)$$

where a and b are constant.

This form of predictive correlation has the same problem as the first form. Moreover, the modification of the relationship from linear to exponential is not supported by theory.

Combination of Dimensionless Terms

For this case, Researchers summarized the factors related to minimum fluidization velocity, grouped them into dimensionless terms, and assembled these terms together based on literature data. R. Coltters and A.L. Rivas [12] even specialized the coefficient according to different materials, particle size, particle density, particle

shape, and different gas. They also emphasized the importance of the properties of the particle surface in U_{mf} prediction. This method is more experimentally based and cannot be explained theoretically.

Literature Data for Minimum Fluidization Velocity and Sphericity

Literature data for minimum fluidization velocity, voidage, and sphericity are listed in Table 2-2 and Table 2-3, along with density and diameter information. Because particle shape is one of the main factors of study, most literature data presented were chosen from non-spherical particles. Figure 2- 2 showed the particles' Geldart's classification of literature data.

Previous Correlation between Voidage and Sphericity

F. Benyahia etc. [13] studied the relationship between voidage and sphericity, and summarized their relationship as stated in Eq. 2-15.

$$\varepsilon_m = 1.504 + \frac{0.2024}{\Phi} \qquad (2\text{-}15)$$

This equation is only valid for $0.42 < \Phi < 1.0$. The extra term related to wall effect has been eliminated. H. Hartman etc. worked out another equation to describe voidage and sphericity (Eq. 2-16) by fitting the literature data.

$$\varepsilon_m = 1.00 - 0.8648\Phi + 0.2745\Phi^2 \qquad (2\text{-}16)$$

In addition, one of the assumptions made by Wen and Yu, which has been proven more accurate [14], also describes the relationship between voidage and sphericity. As illustrated in Figure 2-3, it can be concluded that as sphericity increases, voidage decreases. However, the relation between voidage and sphericity cannot be expressed precisely with a function, as each value of sphericity corresponds to more than one value of voidage.

Objectives of This Study

Because the coefficients in the Ergun equation and the Carman-Kozeny equation are obtained from experimental data, we have reason to believe these coefficients are not perfectly accurate. Nevertheless, the basic format of these equations has been theoretically proven and is convincing. In order to estimate the minimum fluidization velocity with more reliability and less difficulty, we propose to use the Carman-Kozeny equation and replace the $\frac{(1-\varepsilon_m)}{\Phi^2 {\varepsilon_m}^3}$ term and the constant preceding this term with a function of Φ. In this way, we can save the effort of finding ε_m, which is hard to estimate without doing an experiment. This is true because ε_m needs to be experimentally acquired at minimum fluidization velocity, and if an experiment needs to be conducted, then there is no need to work on prediction correlation.

In order to make this modification, we need to study the relationship between voidage and sphericity and examine why the voidage range exists, identifying the parameters that affect voidage. None of existing correlations discussed for this situation are taken into consideration. The goal of this study is to determine the possible parameters that affect voidage of particles with the same sphericity. For particles with a sphericity of close to 1, their shape is quite uniform. However, for cylinders, the sphericity maximizes to 0.87 when the aspect ratio is equal to 1, and then sphericity drops with either an increasing or a decreasing aspect ratio. As shown in Figure 2-4, cylinders with aspect ratio of 0.2 and 5 share an identical sphericity of 0.7, but one of them is a flat disk while the other is a long cylinder. The shape difference becomes more severe as sphericity decreases.

The objectives of this study are as follows:

- To analyze the mechanism of fluidization of spherical and non-spherical particles and to understand the effects of voidage
- To investigate the effects of particle properties and fluidized bed parameters on the voidage and minimum fluidization velocity
- To study the fluidization behavior and voidage of flakes for a better understanding of the fluidization of low sphericity particles

Table 2-1. Prediction correlation of minimum fluidization velocity

Authors	Prediction Correlations
P. Bourgeois, P. Grenier [15]	$Re_{mf} = [(25.46)^2 + 0.0382Ar]^{0.5} - 25.46$
J.F. Richardson, M.A.D.S. Jeromino [16]	$Re_{mf} = [(25.7)^2 + 0.0365Ar]^{0.5} - 25.7$
D.C. Chitester, R.M. Kornosky, L.S. Fan, J.P. Danko [17]	$Re_{mf} = [(28.7)^2 + 0.0494Ar]^{0.5} - 28.7$
J. Reina, E. Velo, L. Puigjaner [18]	$Re_{mf} = [(48)^2 + 0.045Ar]^{0.5} - 48$

Table 2-2. Literature Data for U_{mf} and ε_{mf}

Author	Materials	ρ_p (kg/m^3)	d_p (μm)	Φ_s (-)	U_{mf} (m/s×10^2)	ε_{mf} (-)
S.K. Gupta, V.K. Agarwal, S.N. Singh, et. al. [19]	Iron ore tailings	2551	24.15	0.67	8.34	0.565
	Zinc slime	2748	18.15	0.59	6.78	0.63
	Pre-hydrocyclone uranium tailings	2830	18.62	0.54	7.83	0.654
	Post-hydrocyclone uranium tailings	2677	16.68	0.47	5.73	0.686
	Fly ash	1622	108	0.83	2.51	0.59
Z.Lj. Arsenijevic, Z.B. Grbavcic, R.V. Garic-Gaulovic, F.K. Zdanski [20]	Crushed Stone	2712	2000	0.72	723	0.471
	Crushed Stone	2712	2410	0.697	775	0.467
	Crushed Stone	2712	2730	0.734	813	0.471
A.W. Nienow, P.N. Rowe, L.Y.L Cheung [21]	Copper shot	8860	550	1	49.5	-
	Copper shot	8860	461	1	45.1	-
	Copper shot	8860	273	1	19.5	-
	Copper shot	8860	115	1	4.2	-
	Copper shot	8860	97	1	2.9	-
	Copper shot	8860	70	1	2.3	-
	Copper powder	8860	461	0.56	44.8	-
	Copper powder	8860	273	0.56	16.5	-
	Copper powder	8860	195	0.56	13.5	-
	Bronze shot	8540	388	1	31.5	-
	Bronze shot	8540	273	1	19.5	-
	Bronze shot	8540	231	1	18	-
	Bronze shot	8540	114	1	5.6	-
	Steel shot	7440	388	1	35.2	-
	Steel shot	7440	324	1	26.7	-
	Steel shot	7440	273	1	22.8	-
	Steel shot	7440	138	1	18.1	-

Table 2-2. Continued

Author	Materials	ρ_p (kg/m^3)	d_p (μm)	Φ_s (-)	U_{mf} (m/s×10^2)	ε_{mf} (-)
	Ballotini	2950	550	1	24	-
	Ballotini	2950	461	1	20.3	-
	Ballotini	2950	388	1	18.7	-
	Ballotini	2950	273	1	7.2	-
	Ballotini	2950	231	1	4.3	-
	Ballotini	2950	165	1	3.2	-
	Quartz Glass	2650	273	0.63	9.8	-
	Quartz Glass	2250	388	0.69	11.5	-
	Quartz Glass	2250	324	0.69	10.7	-
	Quartz Glass	2250	273	0.69	6.6	-
A.W. Nienow, P.N. Rowe, L.Y.L Cheung [21]	Sodium perborate	2130	726	0.7	27.4	-
	Carbon	1930	388	0.7	10.8	-
	Carbon	1930	324	0.7	9.7	-
	Carbon	1930	195	0.7	3.4	-
	Sugar	1590	649	0.5	22.4	-
	Sugar	1590	461	0.5	9	-
	Sugar balls	1490	928	1	28.3	-
	Polystyrene spheres	1050	649	1	13.5	-
	Polystyrene spheres	1050	550	1	12.6	-
	Polystyrene spheres	1050	273	1	3.2	-
	Polystyrene spheres	1050	231	1	2.3	-
	Silicon carbide	3220	178	0.67	3.9	0.495
	Silicon carbide	3240	362	0.67	15.6	0.49
	Alumina	4015	259	0.64	10.4	0.51
	Silica sand	2670	167	0.81	2.7	0.44
N.S. Grewal, S.C. Saxena [22]	Silica sand	2670	451	0.84	15.1	0.41
	Silica sand	2670	504	0.88	22	0.42
	Glass beads	2490	265	1	5.9	0.4
	Glass beads	2490	357	1	10.6	0.4
	Glass beads	2490	427	1	16.3	0.405
	Lead glass	4450	241	1	9.3	0.4
	Dolomite	2840	312	0.6	11.8	0.54
	Dolomite	2840	293	0.635	10.5	0.525

Table 2-2. Continued

Author	Materials	ρ_p (kg/m^3)	d_p (μm)	Φ_s (-)	U_{mf} (m/s×10^2)	ε_{mf} (-)
D.S.	Glass spheres	2400	4000	1	171	0.42
Povrenovic,	Glass spheres	2482	5000	1	187	0.43
Dz.E.	Glass spheres	2482	6000	1	208	0.44
Hadzismajlovic, Z.B.	Hollow plastic spheres	529	10000	1	127	0.54
Grbavcic,	Dried peas	1275	5000	1	140	0.44
D.V. Vukovic,	$CaCO_3$	2600	2400	1	115	0.42
H. Littman [23]	Plastic chips	936	3600	0.85	91	0.48
R. Solimene,	Silica Sand	2600	125	~0.8	2.3	-
A.	Silica Sand	2600	328	~0.8	11.1	-
Marzocchella,	Silica Sand	2600	333	~0.8	11.3	-
P. Salatino[24]	Silica Sand	2600	510	~0.8	19.7	-
	Plasticine	1476	7000	1	195.4	0.39
	Plasticine	1476	7125	0.85	178.6	0.335
B. Liu,	Plasticine	1476	7012	0.8	175.1	0.369
X. Zhang,	Plasticine	1476	7019	0.7	173.3	0.382
L. Wang,	Plasticine	1476	6940	0.8	155.2	0.47
H. Hong [25]	Plasticine	1476	7012	0.6	156.8	0.428
	Plasticine	1476	7043	0.6	197.4	0.448
	Plasticine	1476	7000	0.6	168.2	0.512
J. Reina, E. Velo, L. Puigjaner [26]	Forest	621	1140	0.69	25	0.47
	Demolition	759	1480	0.35	32	0.56
	Slot machines	529	1630	0.24	34	0.7
	Furniture	621	1570	0.32	33	0.62
	Palettes	505	1690	0.33	26	0.65
	Carborundum	3180	82	0.92	1.13	0.471
	Carborundum	3180	94	0.95	1.48	0.471
	Carborundum	3180	95	0.94	1.5	0.471
Van Heerden et. al. [27]	Carborundum	3180	117	0.83	2.19	0.496
	Carborundum	3180	162	0.9	4.56	0.487
	Carborundum	3180	192	0.99	5.82	0.476
	Carborundum	3180	225	1	7.09	0.475
	Iron oxide	5180	92	0.88	2.43	0.494

Table 2-3. Literature Data for ε_{mf}

Author	Materials	ρ_p (kg/m^3)	d_p (μm)	Φ_s (-)	U_{mf} (m/s×10^2)	ε_{mf} (-)
M. Leva [28]	Sharp sand	-	50	0.67	-	0.60
	Sharp sand	-	70	0.67	-	0.59
	Sharp sand	-	100	0.67	-	0.58
	Sharp sand	-	200	0.67	-	0.54
	Sharp sand	-	300	0.67	-	0.50
	Sharp sand	-	400	0.67	-	0.49
	Round sand	-	50	0.86	-	0.56
	Round sand	-	70	0.86	-	0.52
	Round sand	-	100	0.86	-	0.48
	Round sand	-	200	0.86	-	0.44
	Round sand	-	300	0.86	-	0.42
	Anthracite coal	-	50	0.63	-	0.62
	Anthracite coal	-	70	0.63	-	0.61
	Anthracite coal	-	100	0.63	-	0.60
	Anthracite coal	-	200	0.63	-	0.56
	Anthracite coal	-	300	0.63	-	0.53
	Anthracite coal	-	400	0.63	-	0.51
	Fischer-Tropsch catalyst	-	100	0.58	-	0.58
	Fischer-Tropsch catalyst	-	200	0.58	-	0.56
	Fischer-Tropsch catalyst	-	300	0.58	-	0.55
G.G. Brown. et al. [29]	Spheres	-	5511.8	1	-	0.3781-0.468
	Glass spheres	-	5308.6	1	-	0.412
	Lead shot, uniform size	-	6350	1	-	0.375 0.375 0.397 0.415 0.421
	Lead shot, uniform size	-	1473.2	1	-	0.363 0.373 0.374 0.375
	Lead shot, uniform size	-	3073.4	1	-	0.370 0.383 0.390

Table 2-3. Continued

Author	Materials	ρ_p (kg/m^3)	d_p (μm)	Φ_s (-)	U_{mf} (m/s×10^2)	ε_{mf} (-)
G.G. Brown. et al. [29]	Celite cylinders	-	6781.8	0.877	-	0.361
						0.365
						0.372
						0.455
						0.457
						0.461
	Celite Spheres	-	5511.8	1	-	0.3784
						0.468
	Berl saddles	-	50038	0.314	-	0.780
		-	35052	0.297	-	0.785
		-	25019	0.317	-	0.750
		-	14986	0.296	-	0.758
		-	11988.8	0.342	-	0.710
		-	9906	0.329	-	0.694
	Berl saddles	-	25400	0.370	-	0.725
	Berl saddles	-	12700	0.370	-	0.7125
						0.761
	Nickel saddles	-	3352.8	0.140	-	0.931
		-	3289.3	0.140	-	0.935
	Raschig rings	-	50038	0.260	-	0.853
		-	35052	0.262	-	0.835
		-	25019	0.272	-	0.826
		-	9906	0.420	-	0.655
	Raschig rings	-	25400	0.391	-	0.707
	Raschig rings	-	9779	0.531	-	0.554
						0.620
	Glass rings	-	5791.2	0.411	-	0.67
		-	6934.2	0.370 (0.314)	-	0.72
		-	9842.5	0.294	-	0.80
		-	11976.1	0.254	-	0.845
	MgO Granules	-	4775.2	0.735	-	0.426
						0.434
						0.513
	Flint sand	-	284.48	0.925	-	0.385
	Glass beads	-	693.42	1.0	-	0.391
	NaCl	-	139.7	0.837	-	0.465

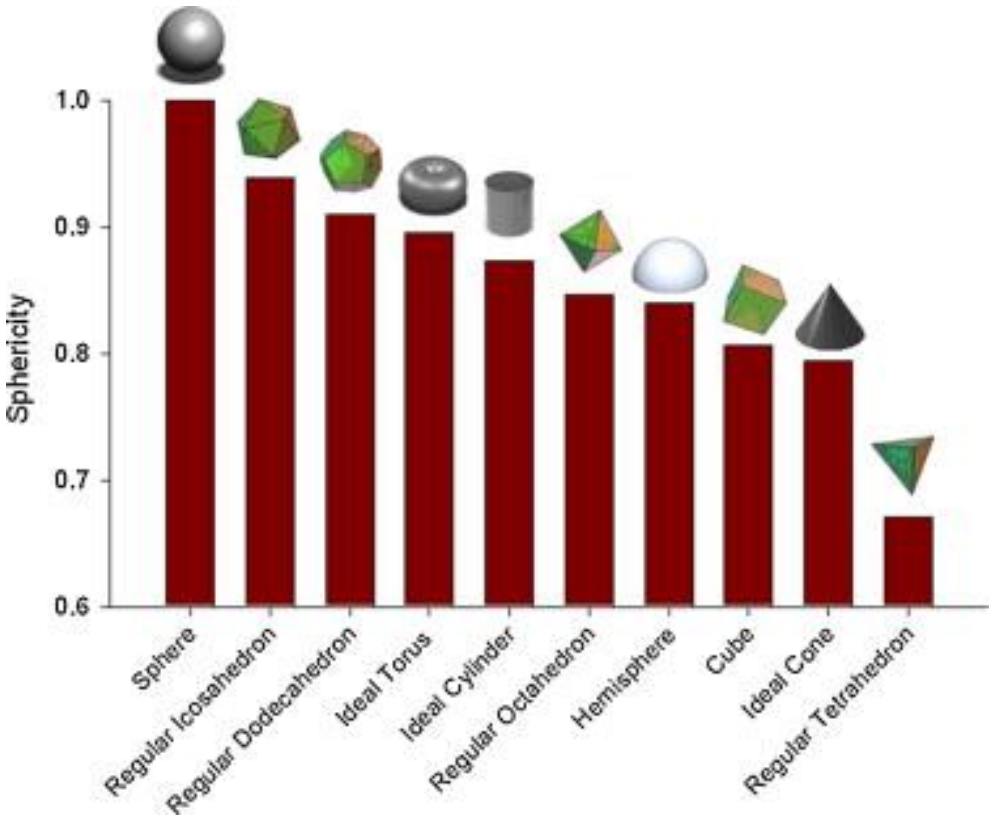

Figure 2-1. A comparison of the sphericity of common 3D objects [8]

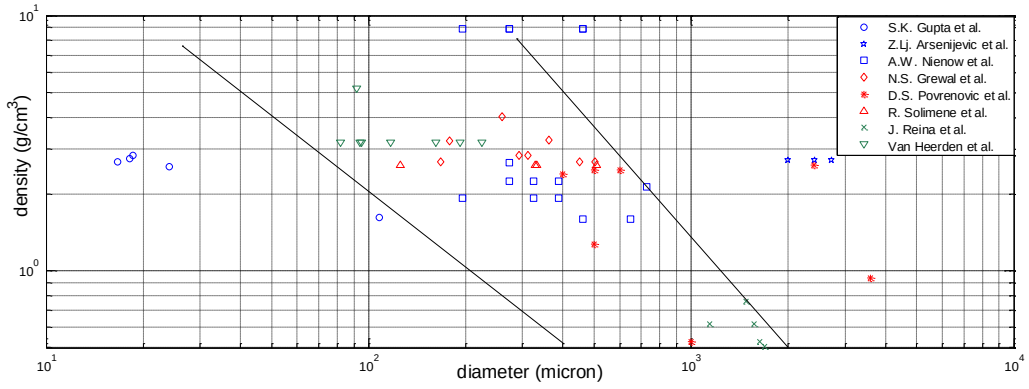

Figure 2-2. Particle Geldart's Classification of literature data

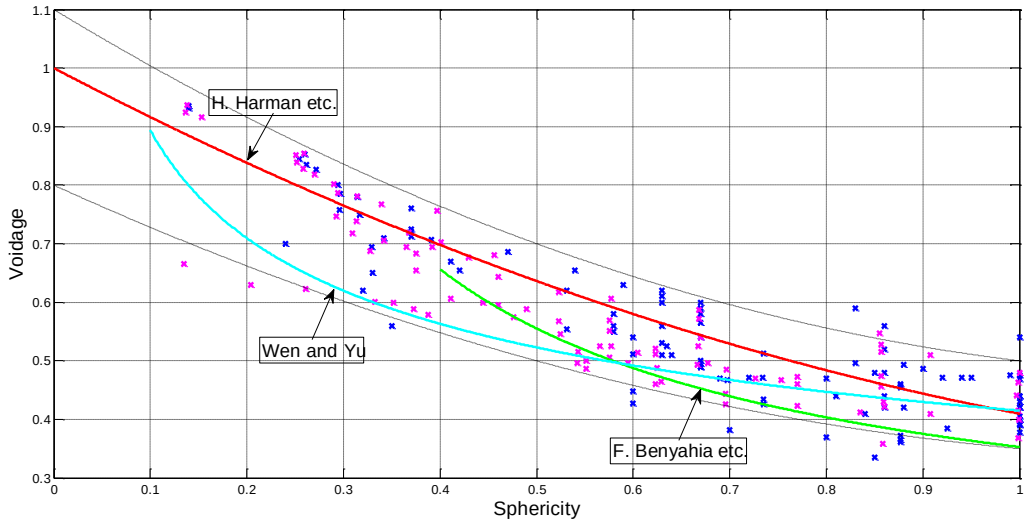

Figure 2-3. Published data and correlation on effect of sphericity on voidage

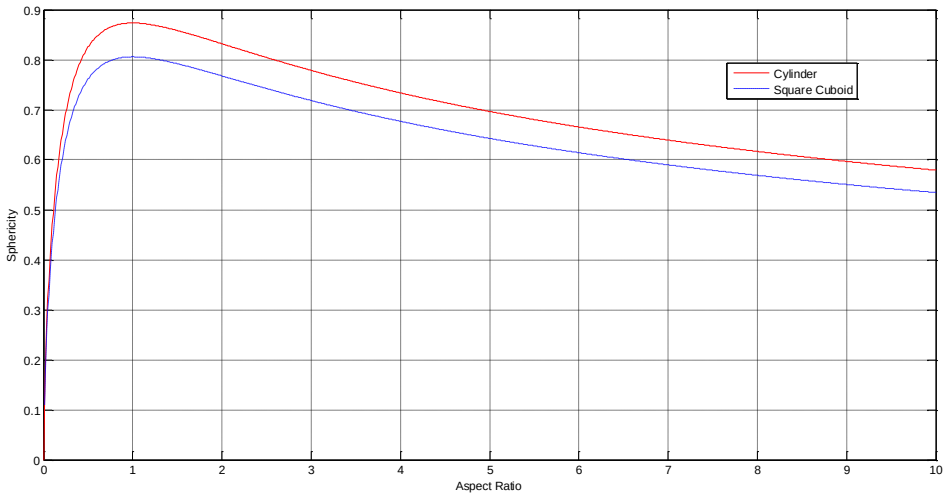

Figure 2-4. Sphericity versus aspect ratio for cylinders and square cuboids

CHAPTER 3
EXPERIMENTAL METHODS

Experimental Materials

In order to study the fluidization behavior of particles with different shapes, 18 particles with different sphericities, ranging from 0.24 to 1.0, were tested in this study. Some materials, such as polyamid cylinders, glass spheres, and flakes, appear well-defined and uniform in shape, while others, such as crushed glass, ovaline, aluminum oxide, and sands, are irregularly shaped. Physical properties of the materials are listed in Table 3-1, and Figure 3-1 shows that all tested particles belong to Geldart's group B.

Density

Density data for all materials were measured with the water displacement method.

Size

Polyamid cylinders and cubes, polycarbonate cylinders, and plastic flakes were manufactured with specific dimensions and a relatively narrow size distribution. However, other materials, like glass spheres, polystyrene spheres, crushed glass, ovaline, aluminum oxide, and sands, varied in their dimensions and had a relatively wide size distribution, so they were sieved manually to achieve a relatively narrow size distribution.

All materials were photographed with an optical microscope-Olympus BX60 digital camera with SPOT insight, using different magnification lenses, and were simultaneously analyzed by ImageJ. Figure 3-2 shows microscope pictures of the spheres. Microscope pictures of the cylinders and cubes can be seen in Figure 3-3. Figure 3-4 shows microscope pictures of the sharp particles. Figure 3-5 contains

microscope pictures of the flakes.For round and sharp particles (with a sphericity of over 0.7), size was also measured by obtaining the equivalent circular area diameter as measured by a BECKMAN COULTER RapidVUE®-Particle Shape and Size Analyzer.

Sphericity

Glass spheres, polystyrene spheres, polyamid cylinders and cubes, polycarbonate cylinders, and plastic flakes are manufactured with a well-defined shape. However, crushed glass, ovaline, aluminum oxide, and sands are not specially manufactured and have irregular shapes. For those materials with a well-defined shape, the sphericity was calculated based on the shape's ideal condition. To achieve the perfect condition, cylinders and cubes were considered to have an aspect ratio equal to 1 and flakes were considered as squares, rectangles, regular diamonds, or regular hexagons. Also, all the particles were treated as monodisperse, which means that they were of a uniform size. For those particles without a well-defined shape, the sphericity was determined by a BECKMAN COULTER RapidVUE®-Particle Shape and Size Analyzer.

Voidage

Voidage at minimum fluidization was calculated based on the following equation (Eq. 3-1)

$$\varepsilon_{mf} = 1 - \frac{m_p}{A \cdot H_{mf} \cdot \rho_p} \qquad (3\text{-}1)$$

where m_p is the weight of the particles, H_{mf} is the height of the fluidized bed at minimum fluidization, ρ_p is the particle density, and A is the cross area of the fluidized bed. Similarly, the height of the static bed was used to calculate the voidage of the static bed, ε_0.

Determination of Experimental Minimum Fluidization Velocity

Experimental minimum fluidization velocity was determined by measuring the pressure drop across a bed of particles. As an example, take the experimental data for glass spheres 400-600 μm: as diagrammed in Figure 3-6, the pressure drop increased with air flow rate until the bed expanded and increased the porosity (blue line). As the air flow rate was further increased, the pressure drop attained a maximum value that was independent of air flow rate. For the fluidization curve of cohesive particles, the value of pressure drop reached a peak and then fell off slightly (as shown in Figure 3-7). This can be expalained, because the frictional force must be overcome before a rearrangement of particles can take place. If the process is reversed, the defluidization line can be obtained (red line). To experimentally identify the minimum fluidization point, a linear function is fitted to the data in the defluidization step before they reach a constant value (as shown in figure 3-6). This line will intersect the constant value of pressure drop for the bed at the minimum fluidization point.

Experimental Apparatus

The air part of GUNT CE 220 Fluidized Bed Formation as shown in Figure 3-8 was used to test minimum fluidization velocity. The inner diameter of the air cylinder vessel is 4.4 cm, and the air flow rate was adjusted and measured by an AAB PurgeMaster A6142C301BNA0DAS with a range of 0-32 L/min.

Experimental Procedure

Before fluidizing the particles, the weight of particles filling the fluidized bed, the initial bed height, the room temperature, and humidity were measured. Then the air flow rate meter was changed at 1 L/min increments until the pressure drop did not varied significantly. At this point, the pressure drop, the flow rate, and the bed height were

recorded. These data belongs to the blue line in figure 3-6. To obtain the defluidization line, shown red in figure 3-6, the flow rate was decreased at the same rate of 1 L/min, and the pressure drop recorded at each point. As an example, the fluidization and defluidization loop of polyamide cylinders is illustrated in Figure 3-7.

Table 3-1. Physical Properties of tested materials

Material	Shape	Dimension (μm)	d_{ev} (μm)	Φ (-)	ρ_p (g/cm^3)
Glass	Spheres	212-300	250 ± 5	1	2.5 ± 0.02
Glass	Spheres	400-600	533 ± 8	1	2.4 ± 0.08
Polystyrene	Spheres	200-400	242 ± 7	1	1.05 ± 0.04
Polystyrene	Spheres	400-600	480 ± 9	1	1.05 ± 0.03
Polycarbonate	Cylinder	500*500 (D*H)	624 ± 7	0.874	1.2 ± 0.02
Polyamid	Cylinder	380*380 (D*H)	451 ± 6	0.874	1.1 ± 0.03
Polyamid	Cylinder	500*500 (D*H)	670 ± 8	0.874	1.1 ± 0.03
Polyamid	Cube	500*500*500	723 ± 6	0.806	1.1 ± 0.03
Ovaline	Irregular	212-300	339 ± 6	0.76	3.4 ± 0.09
Sand	irregular	212-300	281 ± 7	0.75	2.6 ± 0.04
Aluminum Oxide	Irregular	212-300	373 ± 5	0.74	3.9 ± 0.06
Glass	Irregular	212-300	347 ± 9	0.72	2.7 ± 0.05
Glass	Irregular	400-600	630 ± 10	0.72	2.1 ± 0.02
Plastic	Suqare Flake	780*190	604 ± 2	0.63	1.2 ± 0.04
Plastic	Hexagonal Flake	1120*180	654 ± 3	0.60	1.3 ± 0.05
Plastic	Hexagonal Flake	1120*100	538 ± 3	0.46	1.3 ± 0.03
Plastic	Daimond Flake	1500*50	571 ± 5	0.32	1.4 ± 0.02
Plastic	Rectangular Flake	1550*300*40	328 ± 1	0.24	1.4 ± 0.02

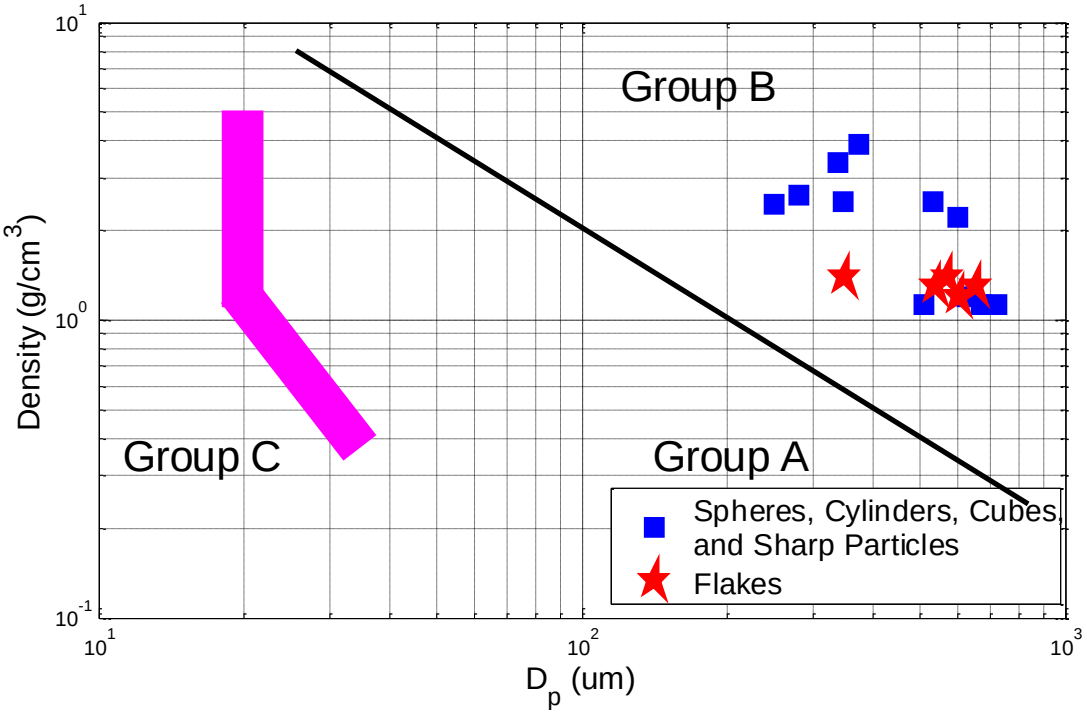

Figure 3-1. Geldart's Group of experimental particles

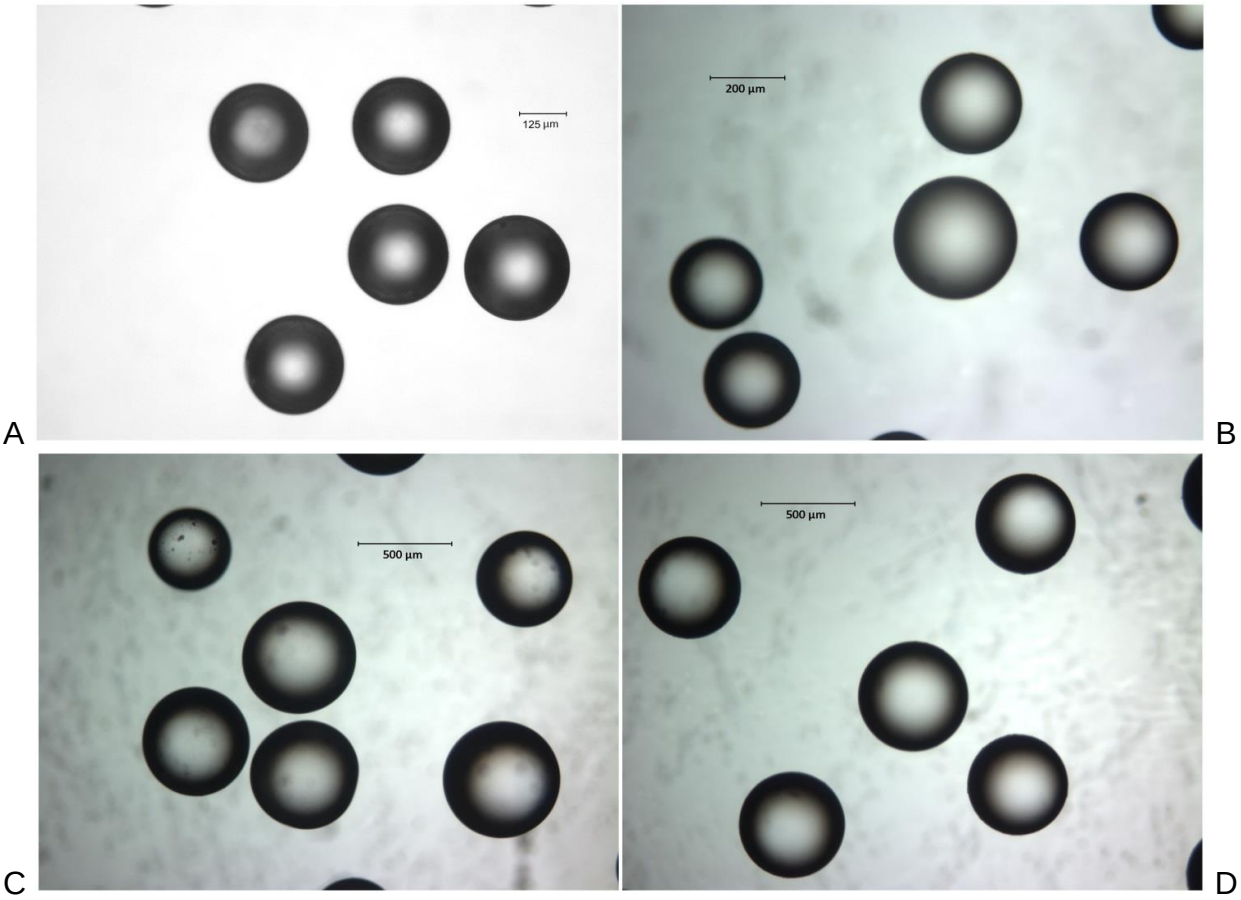

Figure 3-2. Microscope pictures of spheres. A) Glass Spheres 212-300 µm, B) Polystyrene Spheres 200-400 µm, C) Glass Spheres 400-600µm and D) Polystyrene Spheres 425-600 µm.

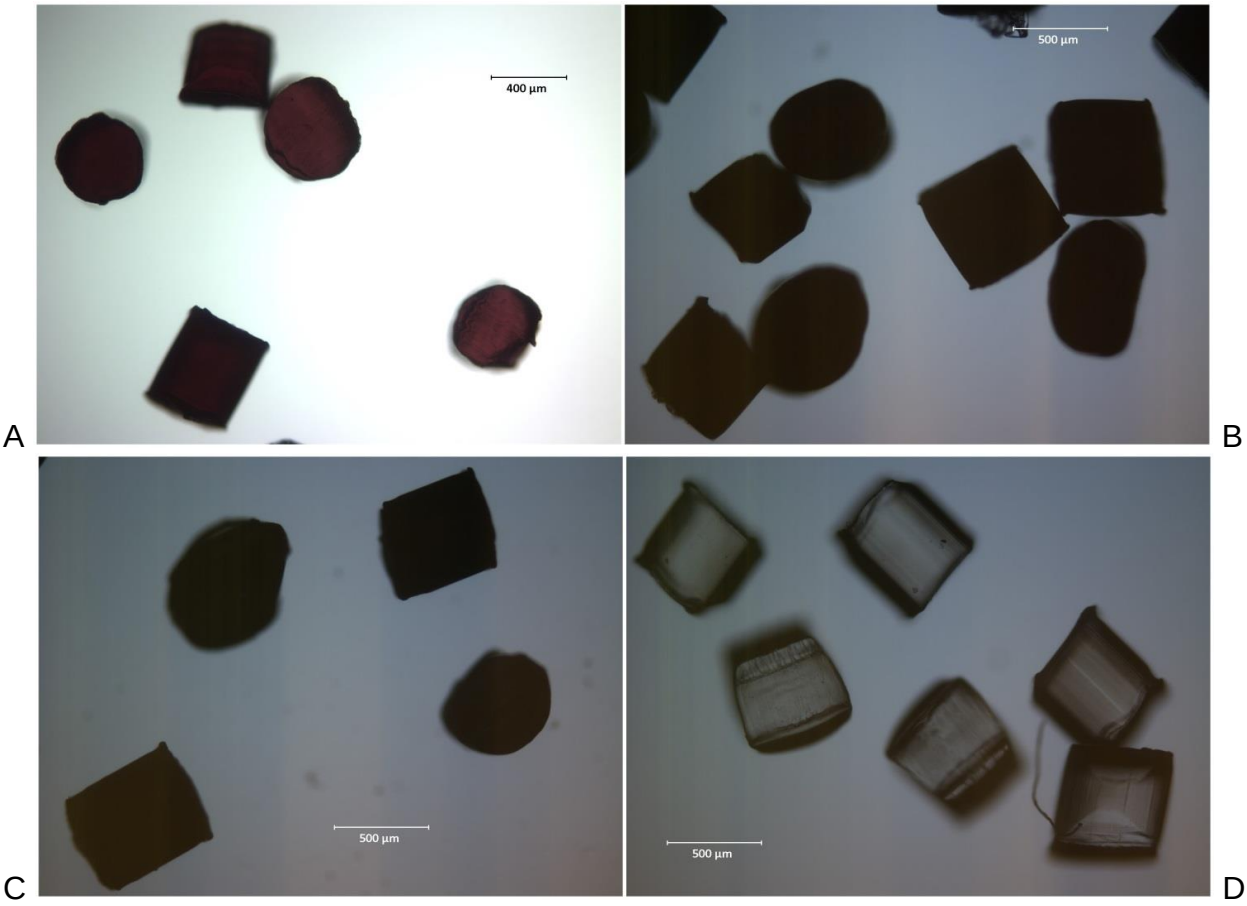

Figure 3-3. Microscope pictures of cylinders and cubes. A) Polyamid Cylinders 380*380 µm, B) Polyamid Cylinders 500*500 µm, C) Polycarbonate Cylinders 500*500 µm and D) Polyamid Cubed 500*500*500 µm.

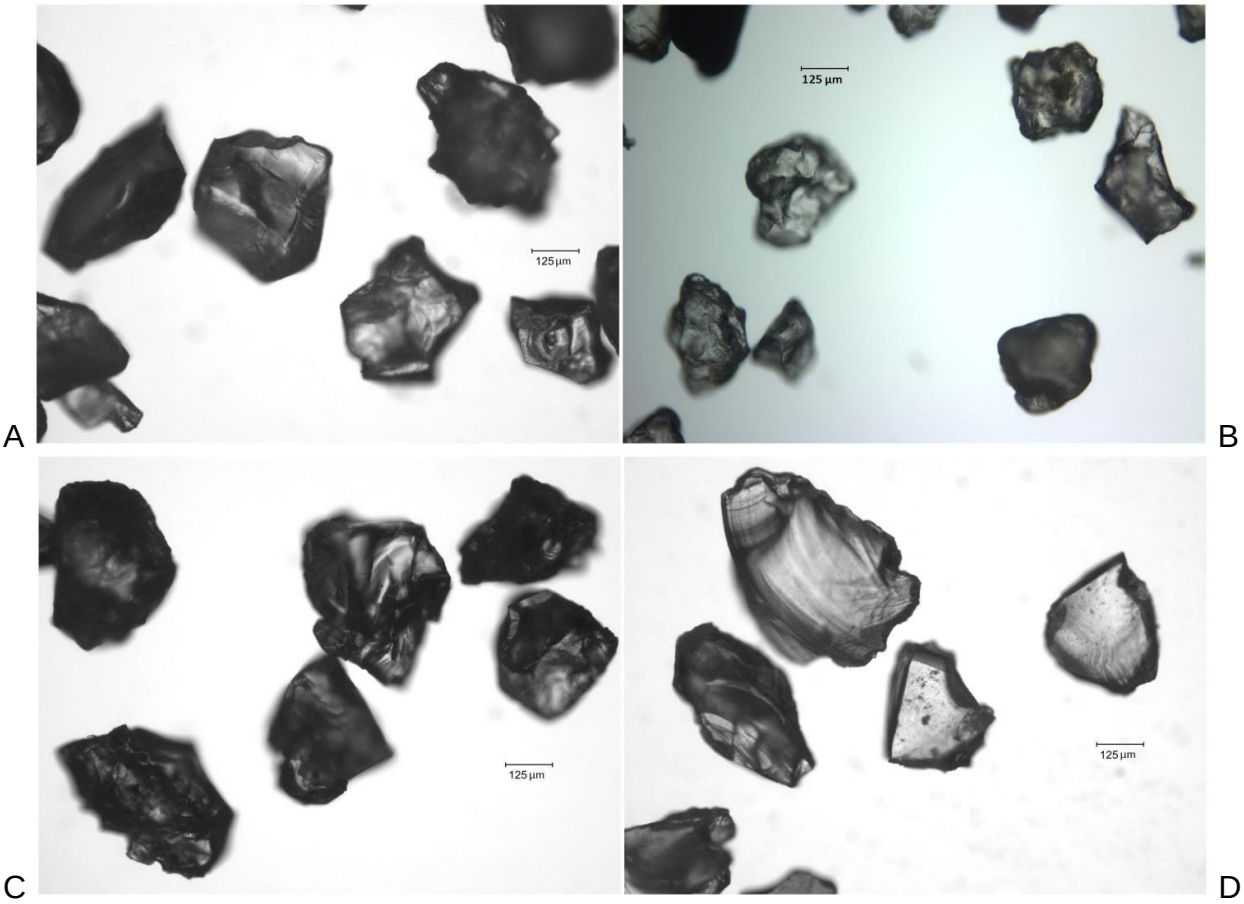

Figure 3-4. Microscope pictures of sharp particles. A) Ovaline 212-300 µm, B) Sand 212-300 µm, C) Aluminum Oxide 212-300 µm and D) P Crushed Glass 212-300 µm.

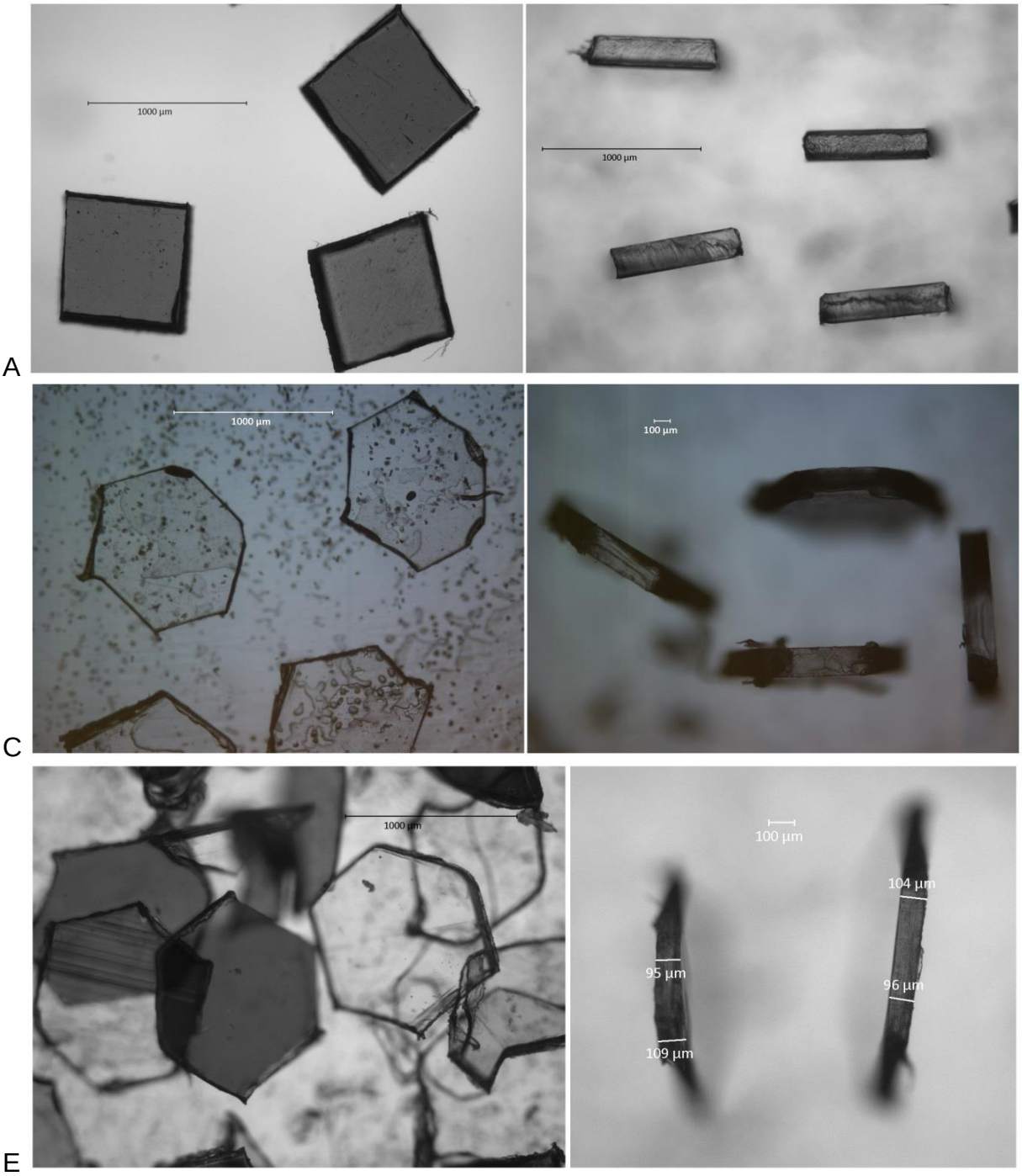

Figure 3-5. Microscope pictures of flakes. A) and B) Plastic Square Flakes 780*190 µm, C) and D) Plastic Hexagonal Flakes 1120*180 µm, E) and F) Plastic Hexagonal Flakes 1120*100 µm.

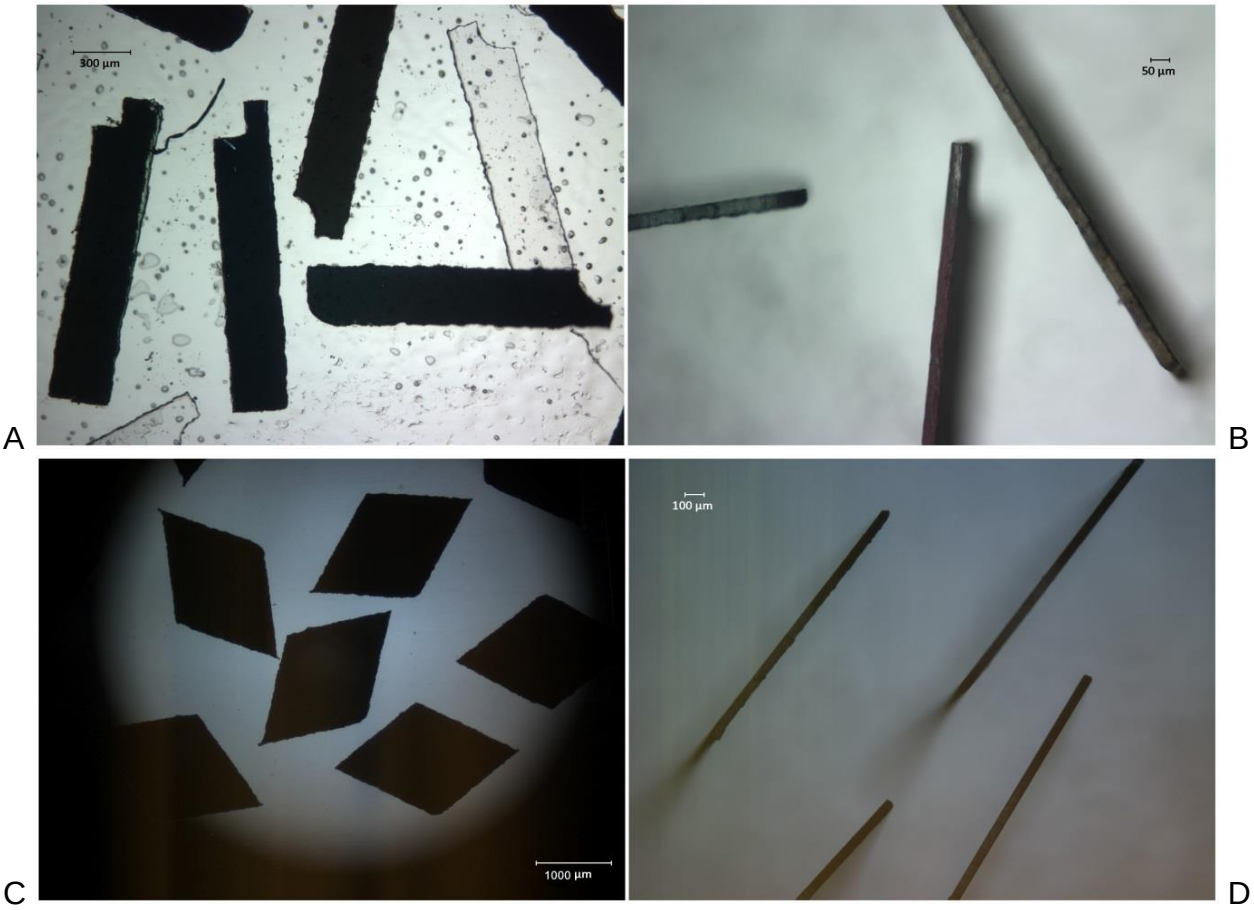

Figure 3-5. Continued. A) and B) Plastic Rectangular Flakes 1550*300*40 µm, C) and D) Plastic Diamond Flakes 1500*50 µm.

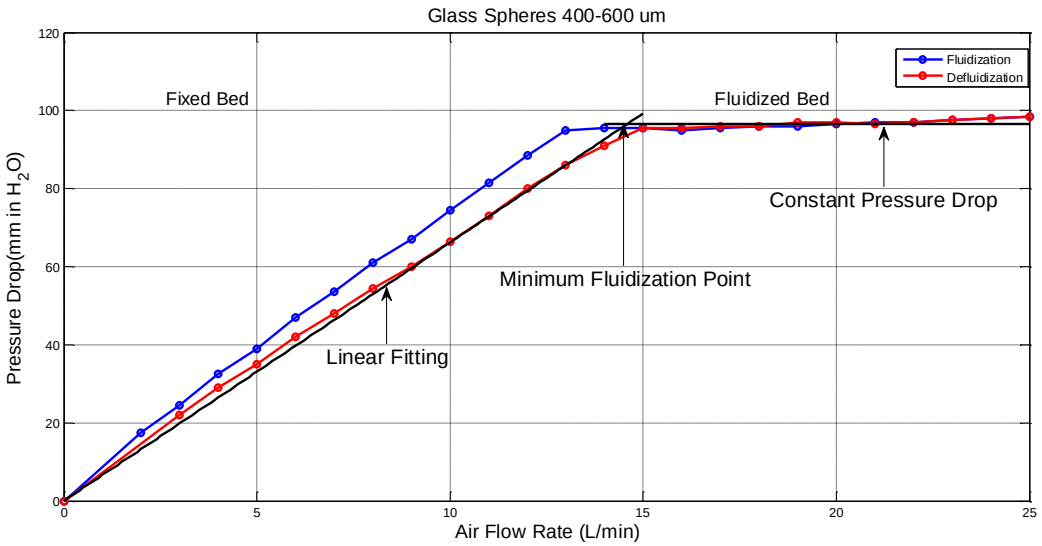

Figure 3-6. Fluidization and defluidization curve of glass spheres 400-600 μm.

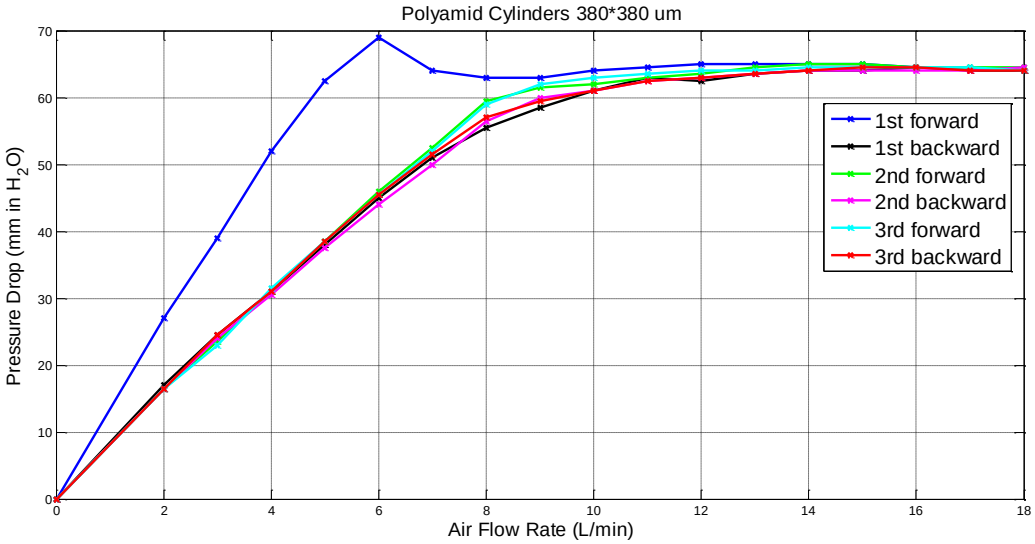

Figure 3-7. Fluidization and defluidization loop of polyamide cylinders 380*380 μm.

A 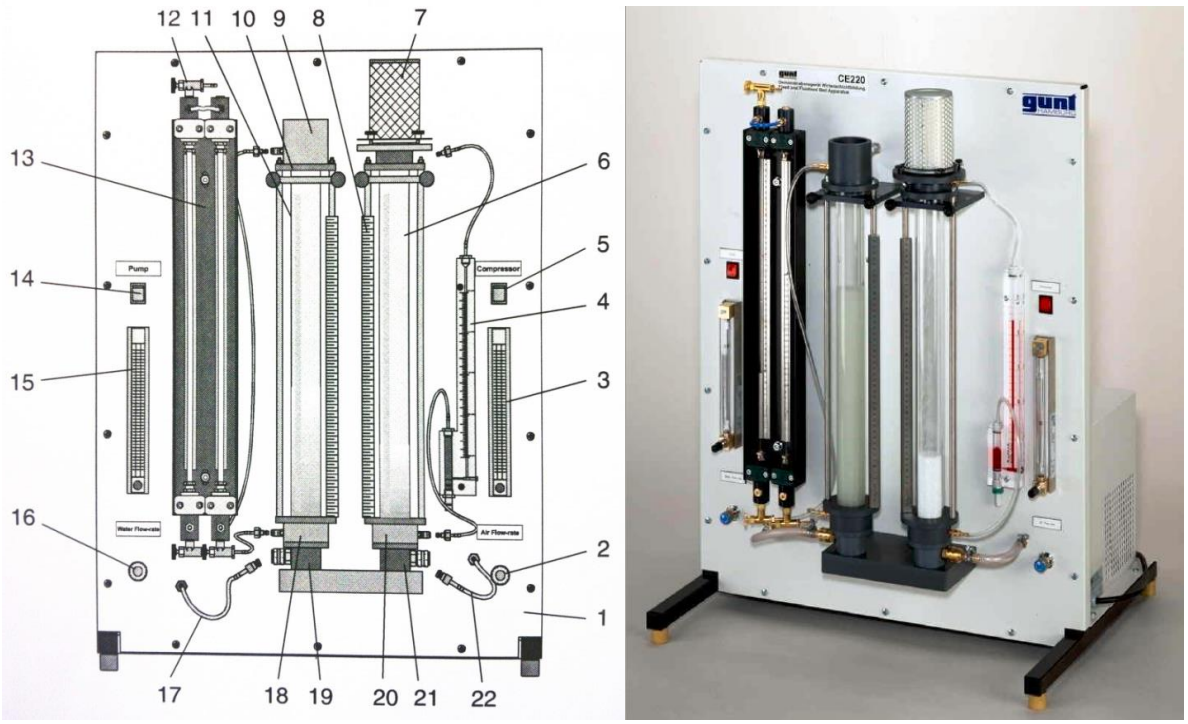

B

Figure 3-8. Schematic diagram of Fluidized Bed GUNT CE 220. A) Schematic layout. B)Picture of Fluidized Bed GUNT CE 220. (Source: http://www.gunt.de/static/s3316_1.php?p1=0&p2=&pN=search;Volltext;ce%20220. Accessed March, 2013.)

1.) Table support with panel; 2.) Bypass valve for air with sound absorber; 3.) Rotameter for air with needle; 4.) Single tube manometer for differential air pressure; 5.) Swith for diaphragm compressor; 6.) Test vessel for air; 7.) Air filter; 8.) Scale; 9.) Water overflow; 10.) Fixing for the upper Sintered plate; 11.) Test vessel for water; 12.) Bleed/vent valve; 13.) Two tube manometer for water pressure; 14.) Switch for diaphragm pump; 15.) Rotameter for water with needle valve; 16.) Bypass valve for water; 17.) Water supply; 18.), 20.) Sintered plate (not visible); 19.), 21.) Distribution chamber; 22.) Air supply. Further components behind the cover (not visible) include: 23.) Supply tank for water with drain tap and safety valve; 24.) Diaphragm pump; 25.) Compressed air reservoir with safety valve; 26.) Diaphragm compressor.

CHAPTER 4
RESULTS AND DISCUSSION

Experimental Results for U_{mf} and ε_{mf}

Table 4-1 shows the experimental results for minimum fluidization velocity and voidage at the minimum fluidization of 16 particles with total particle volume close to 100 cm^3 (with initial bed height around 10 cm). Additionally, Figure 4-1 includes the experimental and literature data for voidage and sphericity.

Explanation for Voidage Range

Voidage was calculated using the theoretical definition. For particles with a fixed dimension and shape, the packing patterns became the main factor influencing voidage. Taking spheres as an example, in a packed bed, for the densest and loosest packing patterns (illustrated in figure 4-2), the voidage can be calculated at 0.27 and 0.48 respectively. Figure 4-2 also shows the densest and loosest packing patterns against the wall, and the voidages are 0.40 and 0.48 respectively. Consequently, different packing patterns of particles can result in different voidages. The same conclusion applies for the non-spherical particles.

Narrowing of Voidage Range Due to Increse in Sphericity

When it comes to voidage, random packing has been emphasized so that the influence of particle packing patterns can be ignored. This policy is more effective for particles with a higher sphericity. For instance, with a fixed packing pattern, no matter how much a sphere was rotated, the voidage of particles in a packed bed or fluidized bed would remain constant. Nevertheless, the orientation of particles with a lower sphericity could significantly affect voidage. A small change in packing patterns could

cause a relatively large difference in voidage. This explains why the voidage range is relatively wider for lower sphericity than it is for higher sphericity.

Factors Accounting for the Voidage Range

Although the voidage range indicates the trend of a change in voidage due to sphericity, this range might result in some error.

The following parameters may account for the range:

- different roughness and cohesion of particles, which can result in different friction forces and aggregations
- different size and wall effect. Different samples of the same material may share the same shape, but those with a larger diameter correspond to lower voidage
- different particle density. Denser particles tend to form a denser packing pattern in fluidized beds, as shown in figure 4-3
- different bed heights. Larger bed heights tend to form a denser packing pattern in fluidized beds, as shown in figure 4-4
- different shapes. Even with same sphericity, the shape can differ based on different aspect ratios

Using sphericity alone to describe the shape of particles is evidently insufficient. For example, in cylinders and square cuboids, sphericity increases and then decreases as aspect ratio increases. In other words, any aspect ratio (other than an aspect ratio equal to 1) can always find another aspect ratio that is its own reciprocal and has the same sphericity, as shown in Figure 2-4. To provide a visual, a disk with a large surface could have the same sphericity as a very long cylinder. However, despite having the same sphericity, the flakes and cylinders have different voidages and behave differently in fluidized beds.

Influence of Bed Height on Voidage and Minimum Fluidization Velocity

The data in Table 4-2 show the influence of different bed heights and particle densities on voidage. As shown in Figures 4-5, 4-6, and 4-7, it can be concluded that voidage decreases as total particle volume increases when $H_{initial}/D_{in}$ <5, and an increase in total particle volume can cause a decrease in U_{mf}. However, this trend weakened as $H_{initial}/D_{in}$ increased, and this could be explained by Janssen's Equation. When bed height increases to a certain point, the vertical forces acting on a particle in a fixed position will no longer change.

Comparison of Experimental Re_{mf} and Theoretical Re_{mf}

The experimental Re_{mf} was calculated based on its definition, as shown in Eq. 2-7, by substituting experimental U_{mf}. Additionally, according to experimental Re_{mf} data, all Re_{mf} are smaller than 10. Hence, it can be implied that they lie in the laminar regime and that the Carman-Kozeny equation is the best one to apply. Through rewriting the Carman-Kozeny equation by substituting the Archimedes number and changing the sequence, the theoretical method used to calculate Re_{mf} can now be expressed as follows (Eq. 4-1):

$$Re_{mf} = \frac{\Phi^2 {\varepsilon_m}^3}{180(1-\varepsilon_m)} Ar \qquad (4\text{-}1)$$

As shown in table 4-3, the theoretical Re_{mf} are larger than those taken from the experiment, ranging from 1.1 to 3.6 times larger. In order to explain the difference, some parameters of particles and the experimental environment were checked. Admittedly, the temperature and humidity of the environment affect the air properties and the sphericity of particles, which contributes to the theoretical Re_{mf}. However, the difference

caused by air density, viscosity, sphericity, and wall effect is relatively small compared to the existing difference.

Half of the tested particles have size ranges bigger than 100 μm, as measured by sieving. However, the equivalent volume diameter measured by the BECKMAN COULTER RapidVUE®-Particle Shape and Size Analyzer is beyond the size range of the particles. Calculating the Re_{mf} for minimum diameter and maximum diameter both experimentally and using Eq. 4-1, the Re_{mf} were more consistent at the minimum diameter values. For cylinders and cubes, the D_{min} was extracted from the average length of each edge, which can be also referred to as the average sieve diameter.

Because Re_{mf} were more consistent at smaller diameters, the smaller particles exerted a larger influence on minimum fluidization than the larger particles. The smaller particles reached a dynamic steady state first. Therefore, the smaller particles were drawn to move upward more readily than the larger particles due to their lower gravitational force, but the smaller particles were resisted by the larger particles above them. Consequently, those smaller particles helped to form a looser packing pattern and increased the voidage at minimum fluidization, which led to a smaller minimum fluidization than expected based on the Re_{mf} calculated using the average diameter.

Fluidization Behavior of Flakes

An interesting phenomenon appeared in the fluidization and defluidization process: when the air flow rate was increased or decreased to slightly below minimum fluidization velocity, small channels appeared against the wall or inside the packed bed, where voidage is relatively high. Air tended to pass through the packed bed through voids with lower resistance. Spheres or particles with a sphericity of close to 1 had higher mobility in the packed or fluidized bed as compared to particles with low

sphericity. Once a channel appeared, particles with higher mobility could react and move quickly to clear channels away. For spheres, those processes happened almost simultaneously without any noticeable channels. On the contrary, for flakes with very low sphericity, due to poor mobility, the channels would remain in place or even continue expanding. Of course, the mobility of particles is not only related to particle shape but also to the roughness of the particle surface.

As illustrated in Figure 4-8, during the fluidization of flakes in a fluidized bed, channeling was observed when the air flow rate was slightly below the minimum fluidization velocity. However, this phenomenon became more obvious as the sphericity of flakes decreased. As shown in Figure 4-9, the pictures were taken before minimum fluidization, when channeling appeared for plastic square flakes and hexagonal flakes. It is evident that the plastic hexagonal flakes 1120*100 μm with a sphericity 0.46, which is lower than the sphericity of the other two flakes, have more apparent channels. Plastic diamond and rectangular flakes with low sphericities (0.24 and 0.36 respectively) could not be fluidized, because deep channels and even cracks appeared as the air flow rate increased, as shown in Figure 4-10.

Effect of Channeling on Minimum Fluidization Velocity

When Ar versus Re_{mf} is plotted with experimental and literature data, as shown in Figure 4-11, flakes can be easily differentiated from other particles because they have a much larger Re_{mf} when Ar is constant. Because Re_{mf} is directly related to U_{mf}, channeling accounts for the large U_{mf}.

New Definition to Describe D_p for Flakes

If the particle diameter D_p is defined as the equivalent volume diameter, then the flakes will fall in the Group B region. However, channels and cracks belong to the

fluidization behavior of Geldart's Group C particles. But if D_p is redefined as the ratio of the volume over the surface area of flakes, the flakes drop to the Group A and C regions. As shown in Figure 4-12, the boundary area of Group A and C may move to a larger D_p region.

The redefinition of D_p as the ratio of the volume over the surface area of flakes keeps the units consistent and also differentiates flakes from long cylinders with the same sphericity. Even though long cylinders were not tested in this research, it is believed that they behave differently in a fluidized bed due to their large differences in shape.

However, this new method of defining D_p may not work for large flakes because D_p will be too high, and therefore they will not fall into the newly defined Group C category. However, experiments with these flakes have not been performed, so it is not known if they will behave as Group A or Group C spherical particles.

Table 4-1. U_{mf} and ε_{mf} data for particles with close particle net volume

Material	Weight (g)	Total Particle Volume (cm^3)	$U_{mf} \pm$ STD (m/s)	ε_0 (-)	$\varepsilon_{mf} \pm$ STD (-)
Glass Spheres 212-300 µm	192.8	78.69	0.0413 ± 0.0002	0.440	0.446 ± 0.005
Glass Spheres 400-600 µm	237.15	95.24	0.156 ± 0.001	0.414	0.417 ± 0.003
Polystyrene Spheres 200-400 µm	100.2	95.43	0.0238 ± 0.0007	0.039	0.444 ± 0.005
Polystyrene Spheres 425-600 µm	98.04	93.37	0.0888 ± 0.0006	0.426	0.432 ± 0.0005
Polycarbonate Cylinders 500*500 µm	114.7	95.58	0.0841 ± 0.003	0.448	0.452 ± 0.003
Polyamid Cylinders 380*380 µm	98.5	87.17	0.0943 ± 0.0008	0.499	0.503 ± 0.0009
Polyamid Cylinders 500*500 µm	101.83	90.12	0.0891 ± 0.0005	0.441	0.445 ± 0.002
Polyamid Cubes 500*500*500 µm	97.6	86.37	0.132 ± 0.002	0.464	0.474 ± 0.0007
Ovaline 212-300 µm	261.4	76.88	0.0700 ± 0.001	0.551	0.556 ± 0.003
Sand 212-300 µm	242.2	91.74	0.0444 ± 0.001	0.531	0.536 ± 0.002
Aluminum Oxide 212-300 µm	260.4	66.77	0.0943 ± 0.001	0.531	0.535 ± 0.0009
Crushed Galss 212-300 µm	200.9	80.36	0.0536 ± 0.0005	0.538	0.542 ± 0.004
Crushed Galss 400-600 µm	183	82.81	0.224 ± 0.009	0.544	0.550 ± 0.001
Plastic Square Flakes 780*190 µm	99.27	82.73	0.2 ± 0.009	0.550	0.561 ± 0.002
Plastic Hexagonal Flakes 1120*180 µm	97.11	74.70	0.173 ± 0.001	0.559	0.568 ± 0.0005
Plastic Hexagonal Flakes 1120*100 µm	68.93	53.02	0.242 ± 0.002	0.719	0.727 ± 0.005

Table 4-2. U_{mf} and ε_{mf} data for particles with different particle net volume

Material	Weight (g)	Total Particle Volume (cm^3)	U_{mf} ± STD (m/s)	ε_0 (-)	ε_{mf} ± STD (-)
Glass Spheres 400-600 µm	148.85	59.78	0.161 ± 0.0006	0.438	0.446 ± 0
	237.15	95.24	0.156 ± 0.001	0.414	0.417 ± 0.003
	349.6	140.4	0.153 ± 0.0006	0.400	0.401 ± 0.002
Polystyrene Spheres 425-600 µm	50.32	47.92	0.0901 ± 0.0003	0.466	0.467 ± 0.001
	98.04	93.37	0.0888 ± 0.0006	0.426	0.432 ± 0.0005
	142.87	136.1	0.0886 ± 0.0002	0.415	0.418 ± 0.0009
Polyamid Cylinders 500*500 µm	51.88	45.91	0.0925 ± 0.0008	0.479	0.483 ± 0.0005
	101.83	90.12	0.0891 ± 0.0005	0.441	0.445 ± 0.002
	202.98	179.6	0.0881 ± 0.0006	0.412	0.419 ± 0.003
Polyamid Cubes 500*500*500 µm	54.1	47.88	0.142 ± 0.005	0.492	0.508 ± 0.005
	97.6	86.37	0.132 ± 0.002	0.464	0.474 ± 0.0007
	194.6	172.2	0.119 ± 0.002	0.434	0.440 ± 0.002
	281.2	248.9	0.118 ± 0.003	0.424	0.431 ± 0.003
	401.45	355.3	0.118 ± 0.001	0.418	0.425 ± 0.002
Hexagonal Flakes 1120*180 µm	47.91	36.85	0.171 ± 0.0009	0.589	0.596 ± 0
	97.11	74.70	0.173 ± 0.001	0.559	0.568 ± 0.0005
	189.84	146.0	0.173 ± 0.0008	0.539	0.550 ± 0.002

Table 4-3. Comparison of Experimental Re_{mf} and Re_{mf} from Carman-Kozeny equation

Material	D_v (μm)	Experimental			Carman-Kozeny Equation		
		$Re_{mf}(D_v)$	$Re_{mf}(D_{min})$	$Re_{mf}(D_{max})$	$Re_{mf}(D_v)$	$Re_{mf}(D_{min})$	$Re_{mf}(D_{max})$
Glass Spheres 212-300 μm	250	0.64	0.54	0.77	1.12	0.68	1.93
Glass Spheres 400-600 μm	533	5.18	3.89	5.83	8.52	3.60	12.15
Polystyrene Spheres 200-400 μm	242	0.36	0.30	0.59	0.43	0.24	1.93
Polystyrene Spheres 425-600 μm	480	2.66	2.35	3.32	3.00	2.08	5.85
Polycarbonate Cylinders 500*500 μm	624	3.27	2.83	-	6.79	4.40	-
Polyamid Cylinders 380*380 μm	451	2.65	2.35	-	3.69	2.58	-
Polyamid Cylinders 500*500 μm	670	3.72	3.11	-	7.50	4.40	-
Polyamid Cubes 500*500*500 μm	723	5.95	5.25	-	10.18	5.75	-
Ovaline 212-300 μm	339	1.48	0.92	1.31	5.39	1.32	3.73
Sand 212-300 μm	281	0.78	0.59	0.83	1.98	0.85	2.41
Aluminum Oxide 212-300 μm	373	2.19	1.25	1.76	6.63	1.22	3.45
Crushed Galss 212-300 μm	347	1.16	0.71	1.00	3.39	0.77	2.19
Crushed Galss 400-600 μm	630	8.79	5.58	8.37	18.97	4.86	16.39
Plastic Square Flakes 780*190 μm	604	7.53	-	-	7.76	-	-
Hexagonal Flakes 1120*180 μm	654	7.05	-	-	10.14	-	-
Hexagonal Flakes 1120*100 μm	538	8.11	-	-	11.07	-	-

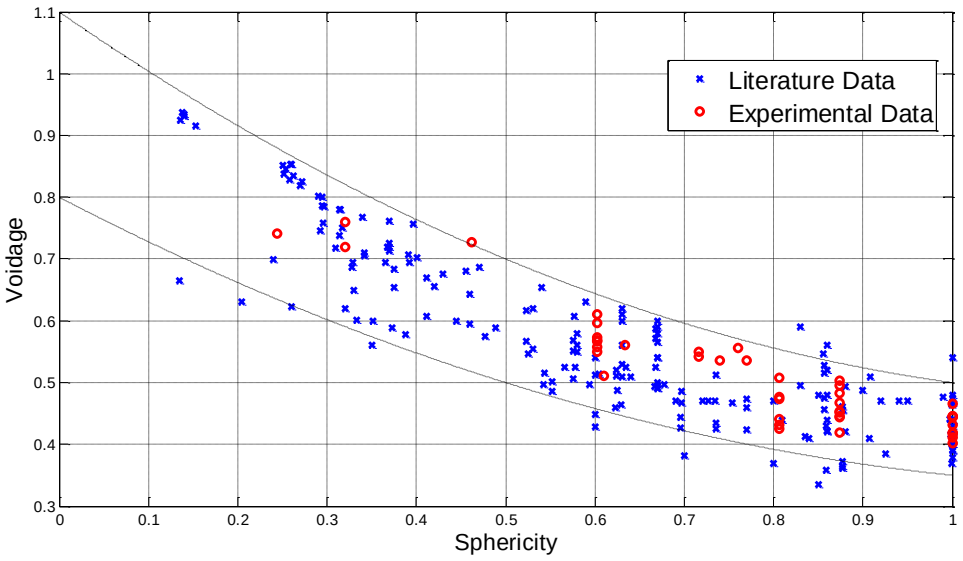

Figure 4-1. Literature data and experimental data of sphericity versus voidage

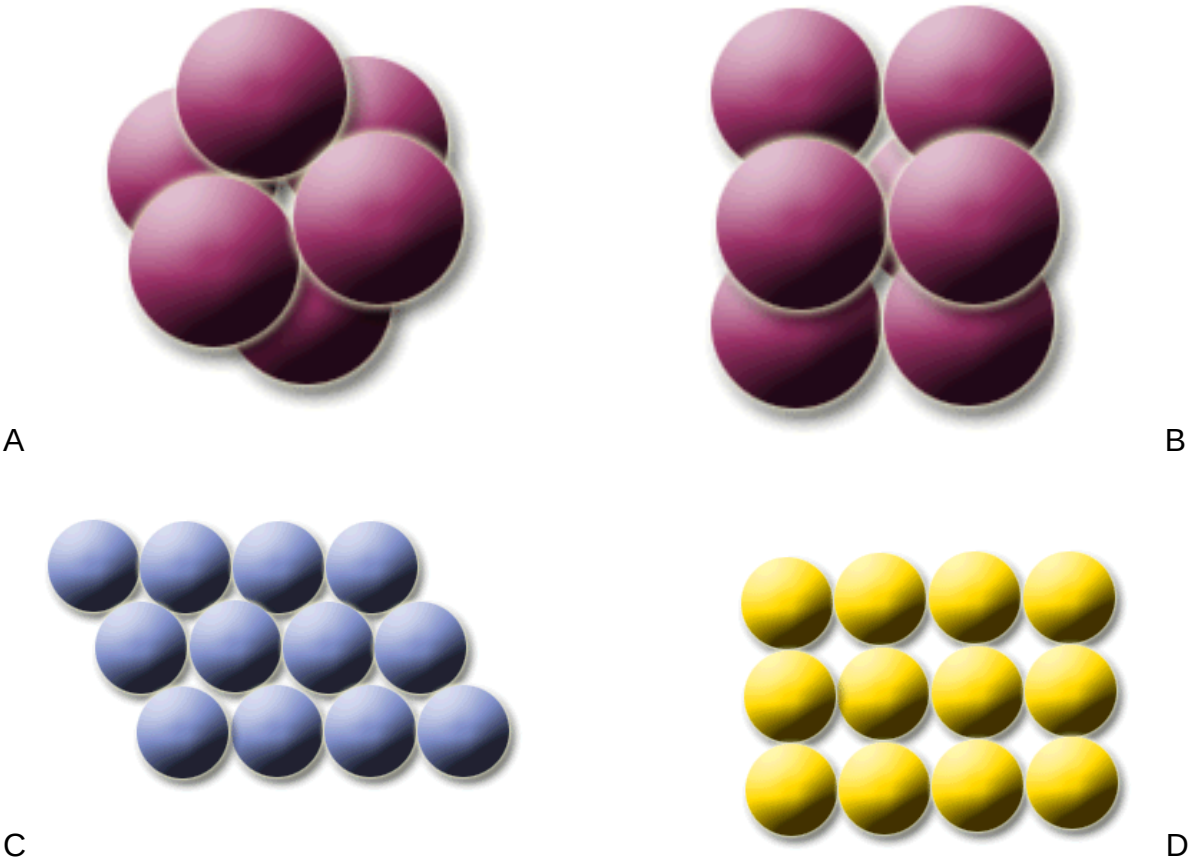

Figure 4-2. Spheres packing. A) densest packing in packed bed, B) Loosest packing in packed bed, C) densest packing against the wall and D) loosest packing against the wall. (Source: http://www.earth360.com/math_spheres.html. Last accessed March, 2013).

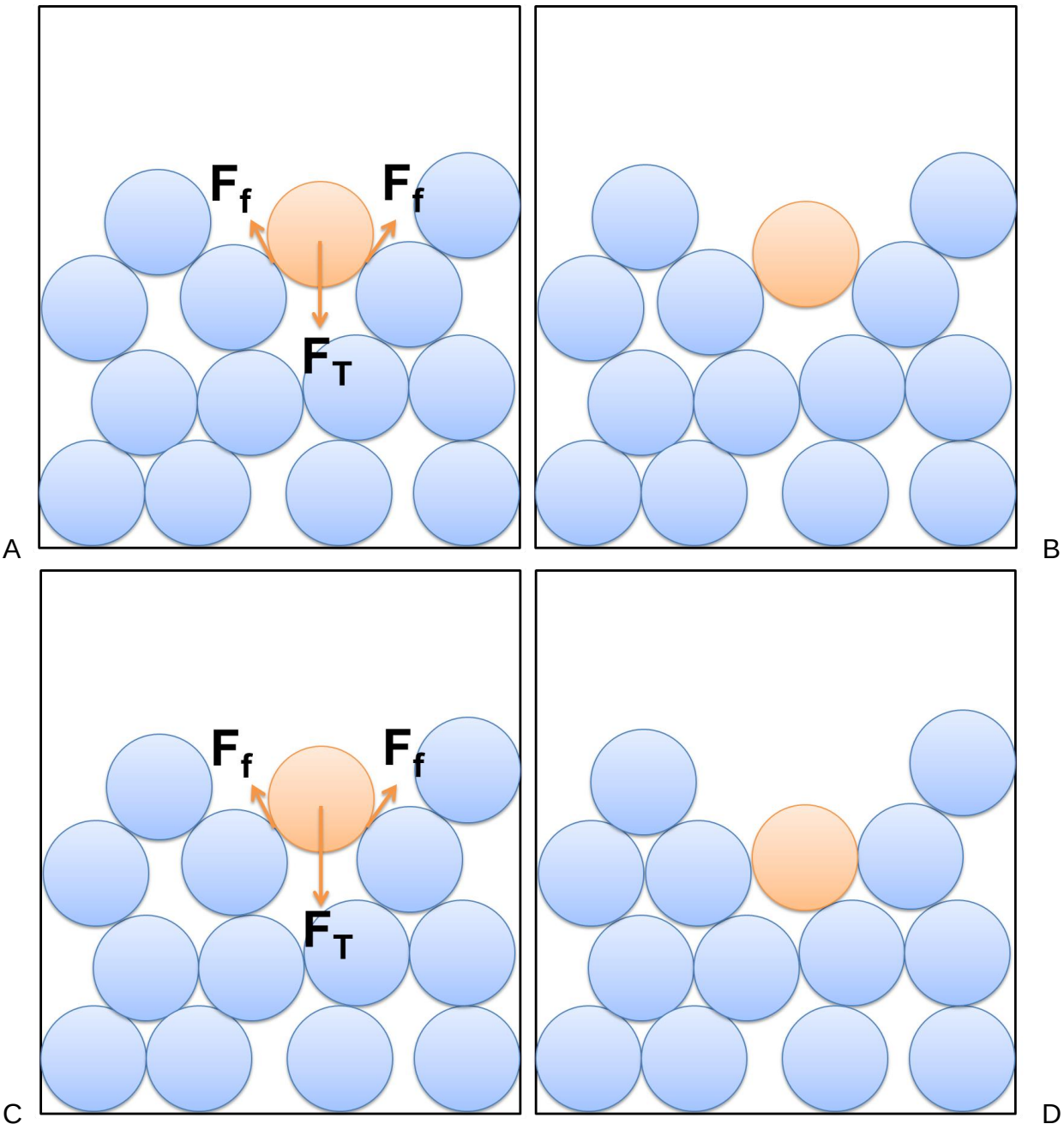

Figure 4-3. Force analysis of single particle with different density in fluidized bed. A) force analysis of single particle in fluidized bed, B) particles with smaller density formed a looser packing, C) force analysis of single particle in fluidized bed and D) particles with larger density formed a denser packing.

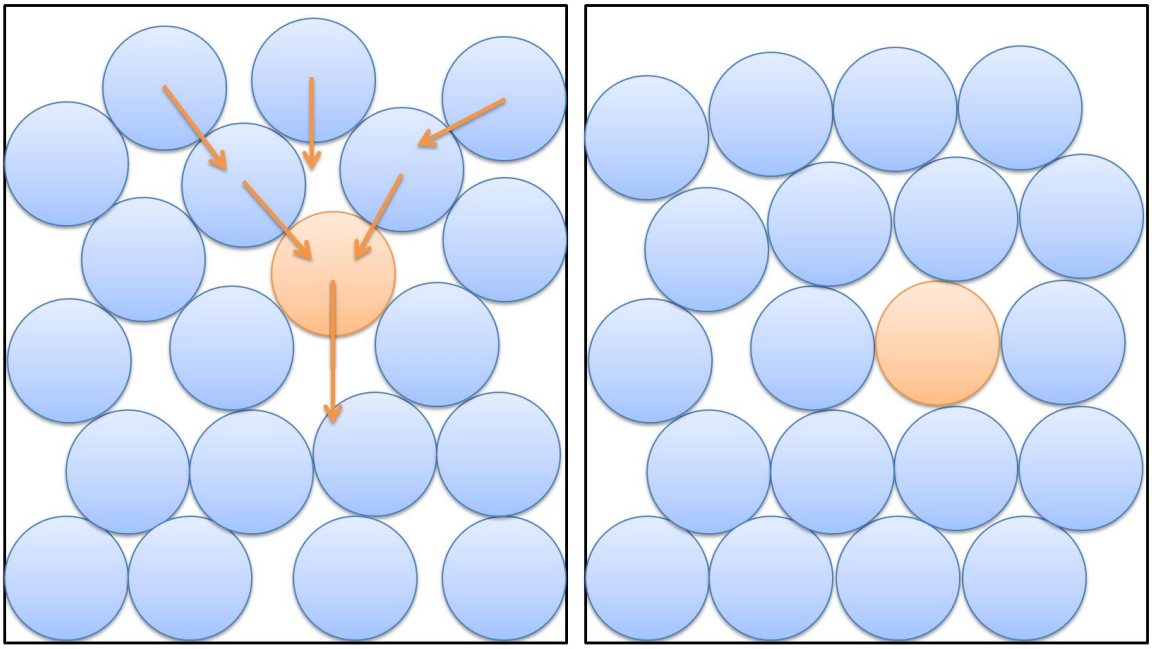

A B

Figure 4-4. Force analysis of single particle with different bed height in fluidized bed. A) force analysis of single particle in fluidized bed, B) particles with larger bed height formed a denser packing.

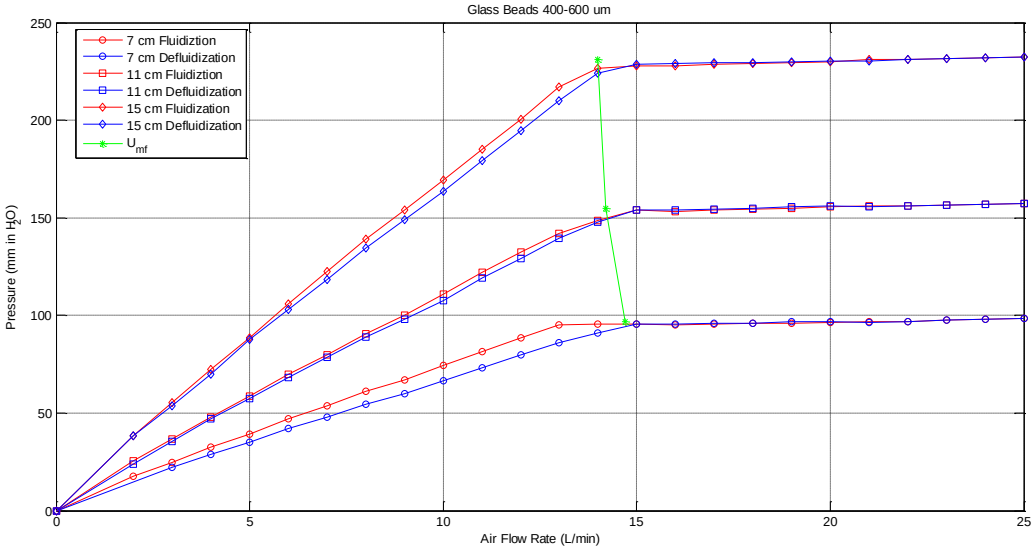

Figure 4-5. Fluidization and Defluidization curve and minimum fluidizaiton veloicity of glass spheres 400-600 μm at different particle total volume (initial bed height).

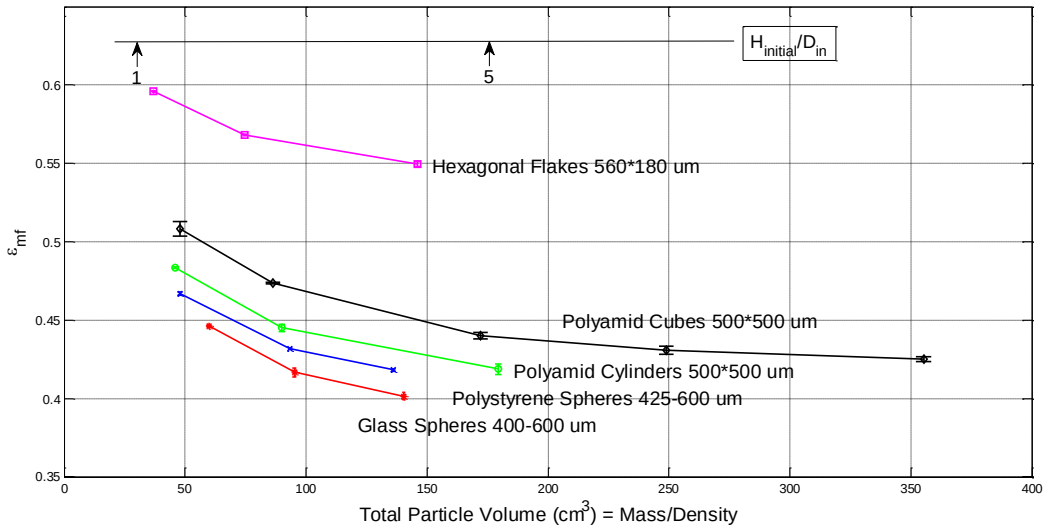

Figure 4-6. Influence of Bed Height on Voidage.

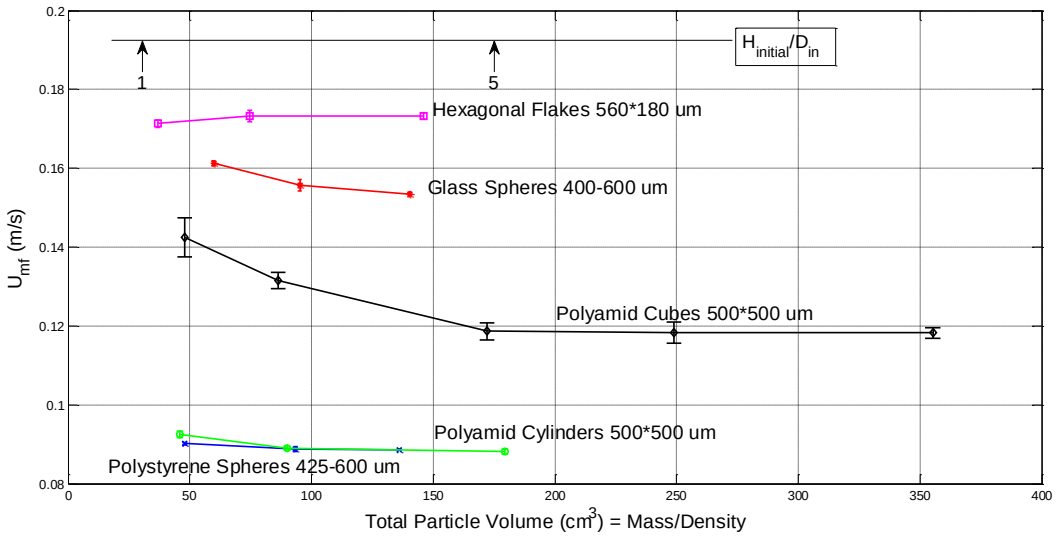

Figure 4-7. Influence of Bed Height on minimum fluidization velocity.

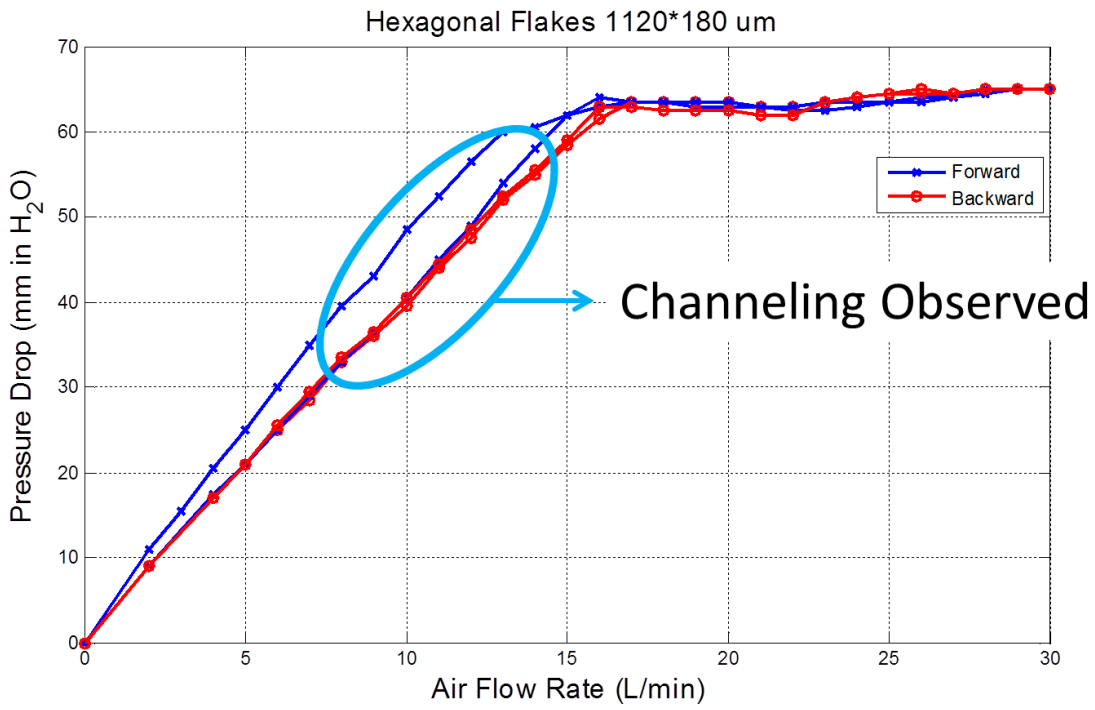

Figure 4-8. Fluidization and Defluidization curve of Hexagonal Flakes 1120*180 µm.

A   B

C 

Figure 4-9. Fluidization behavior of flakes. A) channeling of plastic square flakes 780*190 µm, B) channeling of plastic hexagonal flakes 1120*180 µm and C) channeling of plastic hexagonal flakes 1120*100 µm.

A  B

Figure 4-10. Channeling and cracks of flakes. A) channeling of plastic diamond flakes 1500*50 µm and B) channeling and cracks of plastic rectangular flakes 1550*300*40 µm.

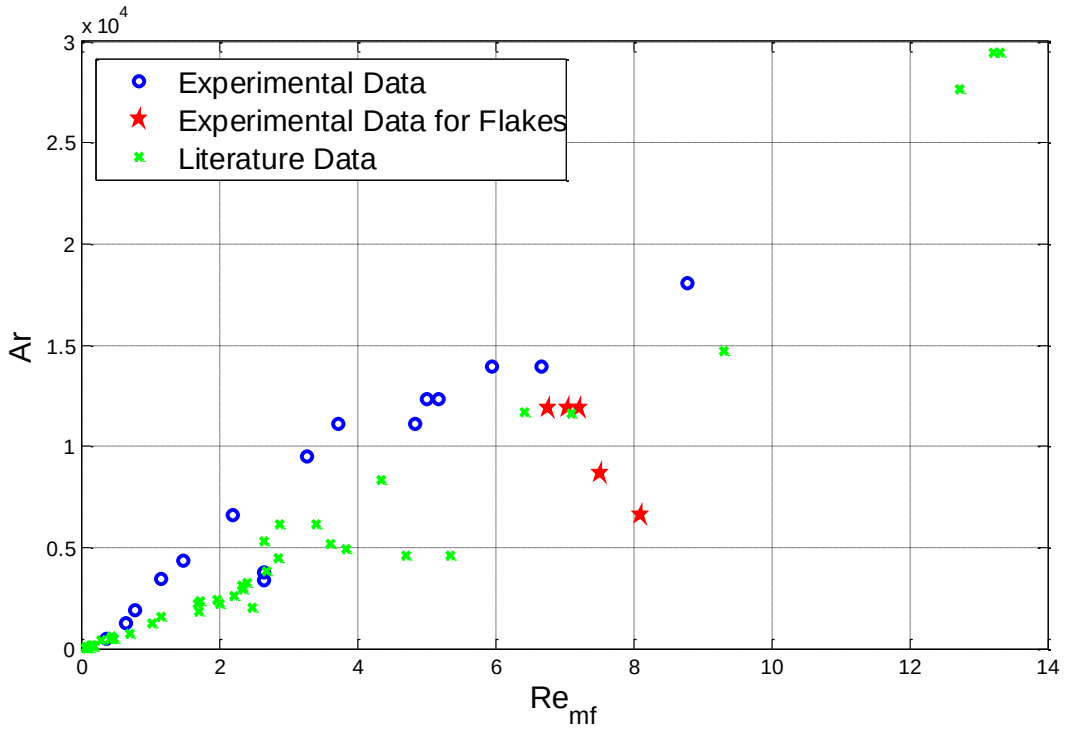

Figure 4-11. Influence of channeling on minimum fluidization velocity.

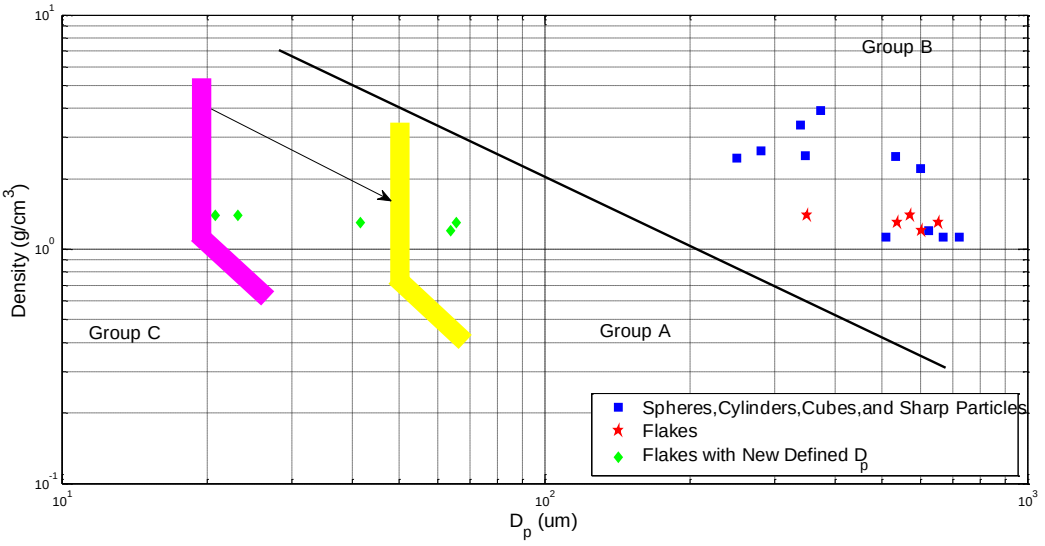

Figure 4-12. Redefine D_p for flakes and boundary for Geldart's Group A and C.

CHAPTER 5
CONCLUSION AND FUTURE WORK

Conclusion

Based on the fluidized bed experiment performed for particles with different shapes, densities, and dimensions, fluidization behavior was investigated and classified. In the process of seeking to explain voidage range, particle density and initial bed height were taken into consideration. The main findings of this work can be summarized as follows:

- When $H_{initial}/D_{in} < 5$, as the total particle volume increases, the voidage decreases, causing a decrease in U_{mf}
- Flakes with a volume/surface area ratio of less than 60 have Geldart's Group C properties

Future Work

It is believed that the fluidization behavior of flakes and elongated particles is quite different from that of spheres when the sphericity is less than a certain value. However, in this study, we have only tested flakes with a sphericity of 0.24 to 0.63 and a thickness of 40 μm to 180 μm. Therefore, we are not sure whether the channeling behavior of flakes is due to shape, thickness, or the roughness of the surface. A better knowledge of this interesting behavior may give us a deeper understanding of the fluidized bed mechanism.

Future work on the fluidization behavior of flakes could focus on the following points:

- To study flakes of different densities and sizes in order to better determine the D_p of flakes and the boundary of Geldart's Group A and Group C in fluidized beds
- To explore the effects of the surface roughness of flakes on the cohesive fluidization behavior

- To investigate the fluidization behavior of elongated cylinders with low sphericity and to examine the differences between flakes and cylinders

APPENDIX
FLUIDIZATION AND DEFLUIDIZATION CURVES OF FLAKES

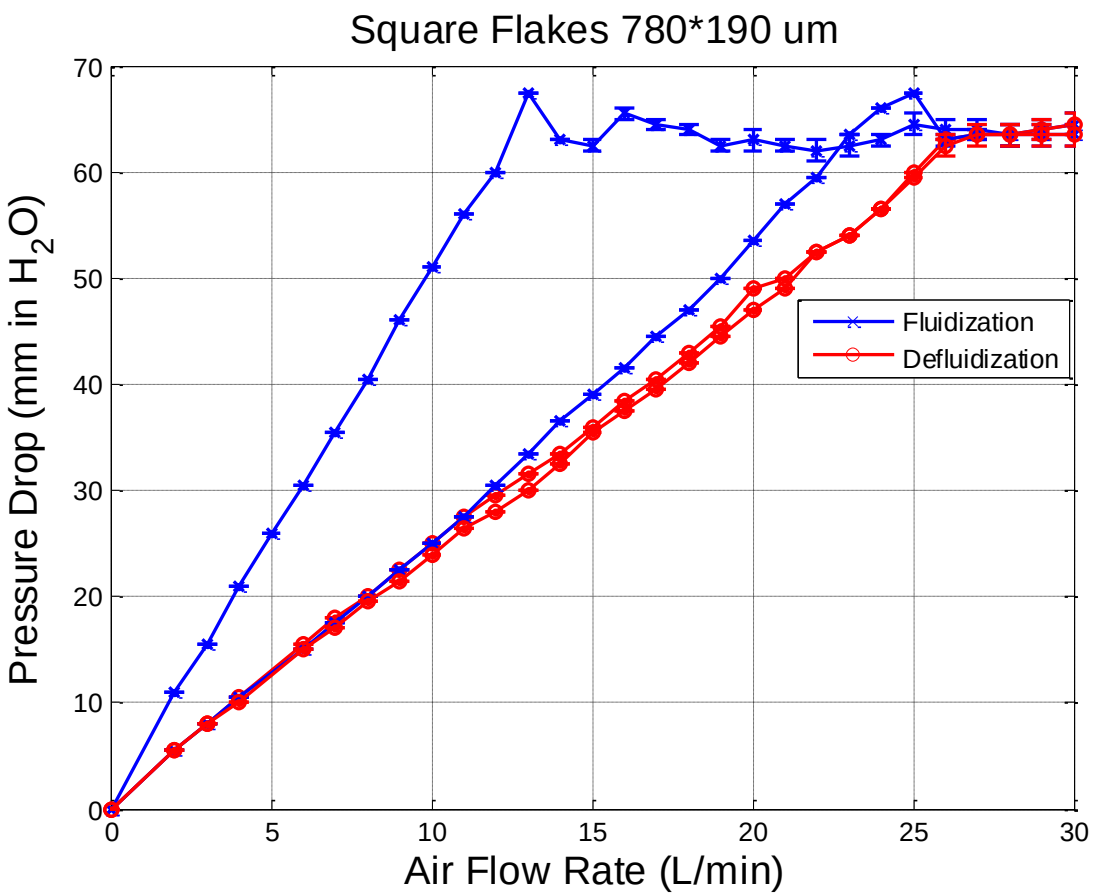

Figure A-1. Fluidization and defluidization curves for plastic square flakes 780*190 μm.

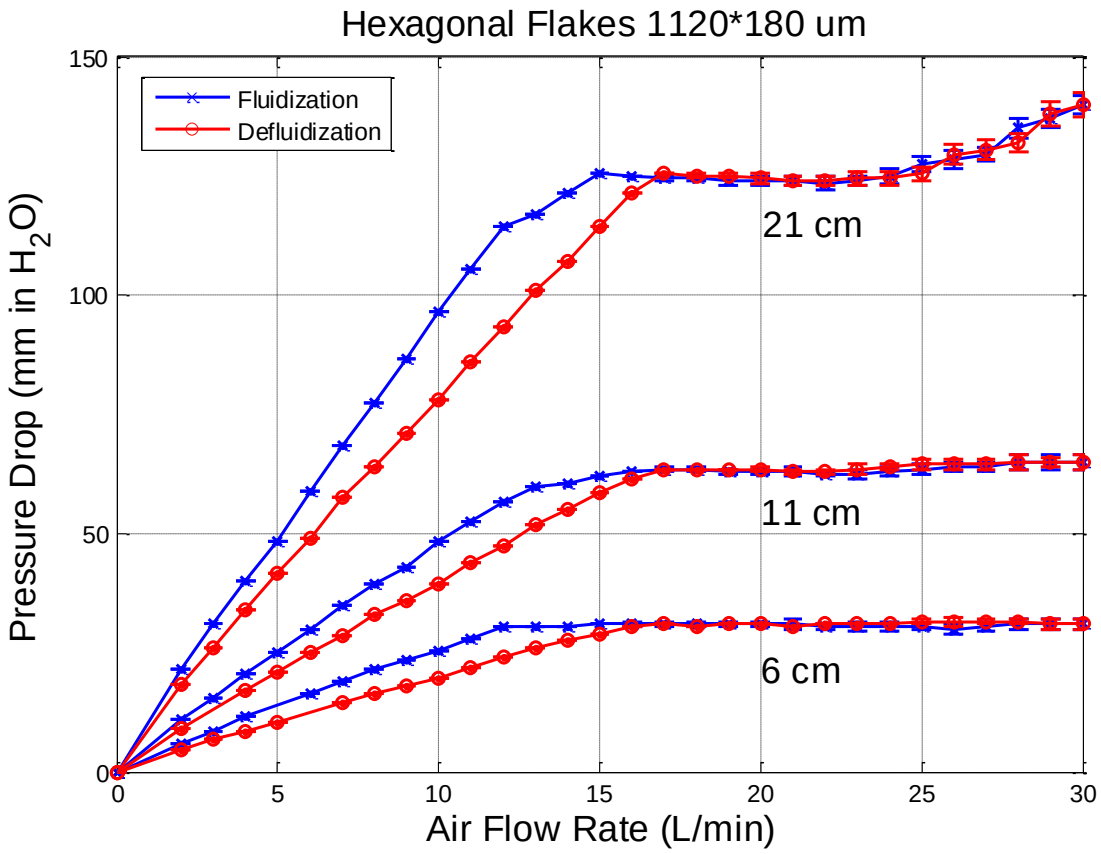

Figure A-2. Fluidization and defluidization curves for plastic hexagonal flakes 1120*180 μm at different initial bed height.

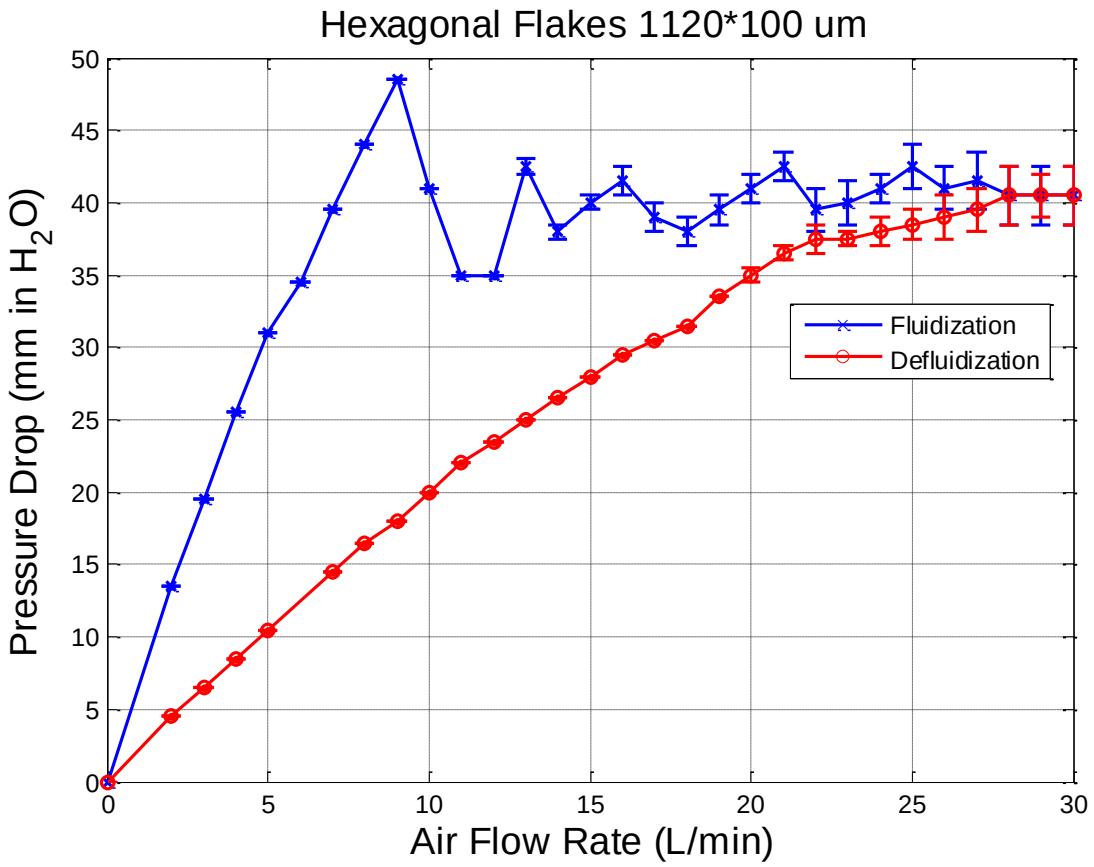

Figure A-3. Fluidization and defluidization curves for plastic hexagonal flakes 1120*100 μm.

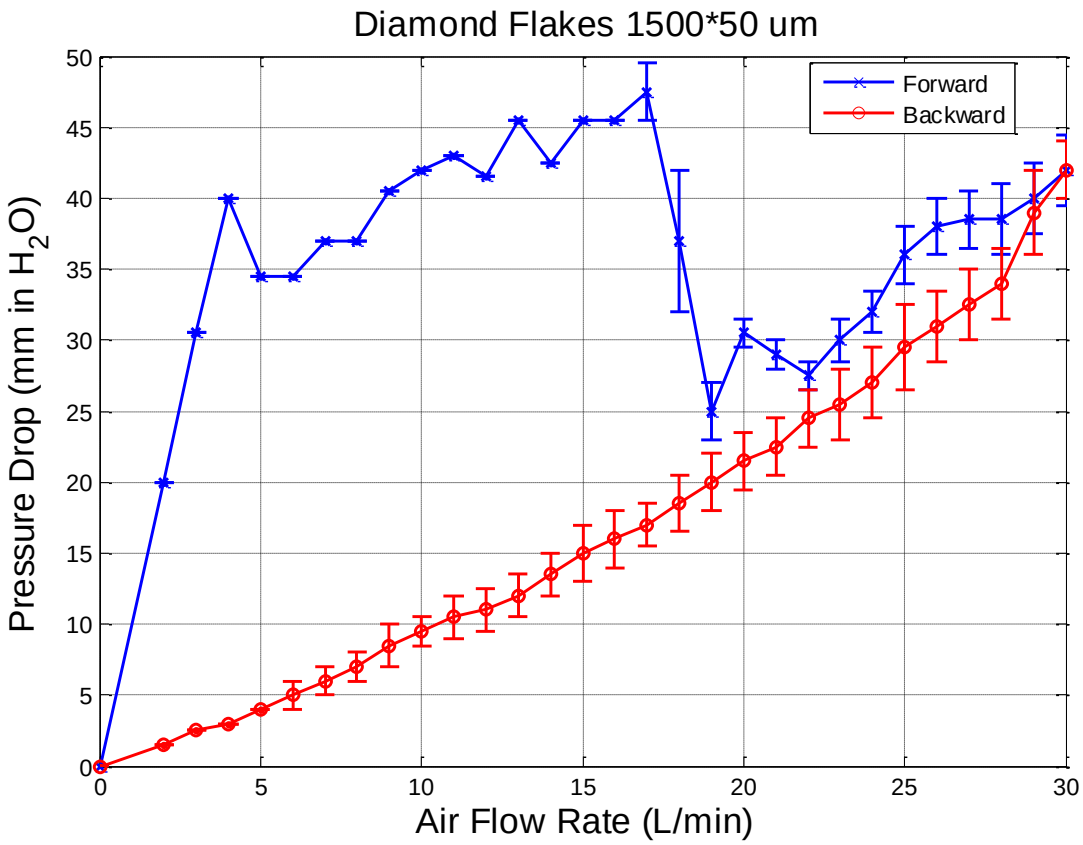

Figure A-4. Pressure drop versus air flow rate for plastic diamond flakes 1500*50 μm.

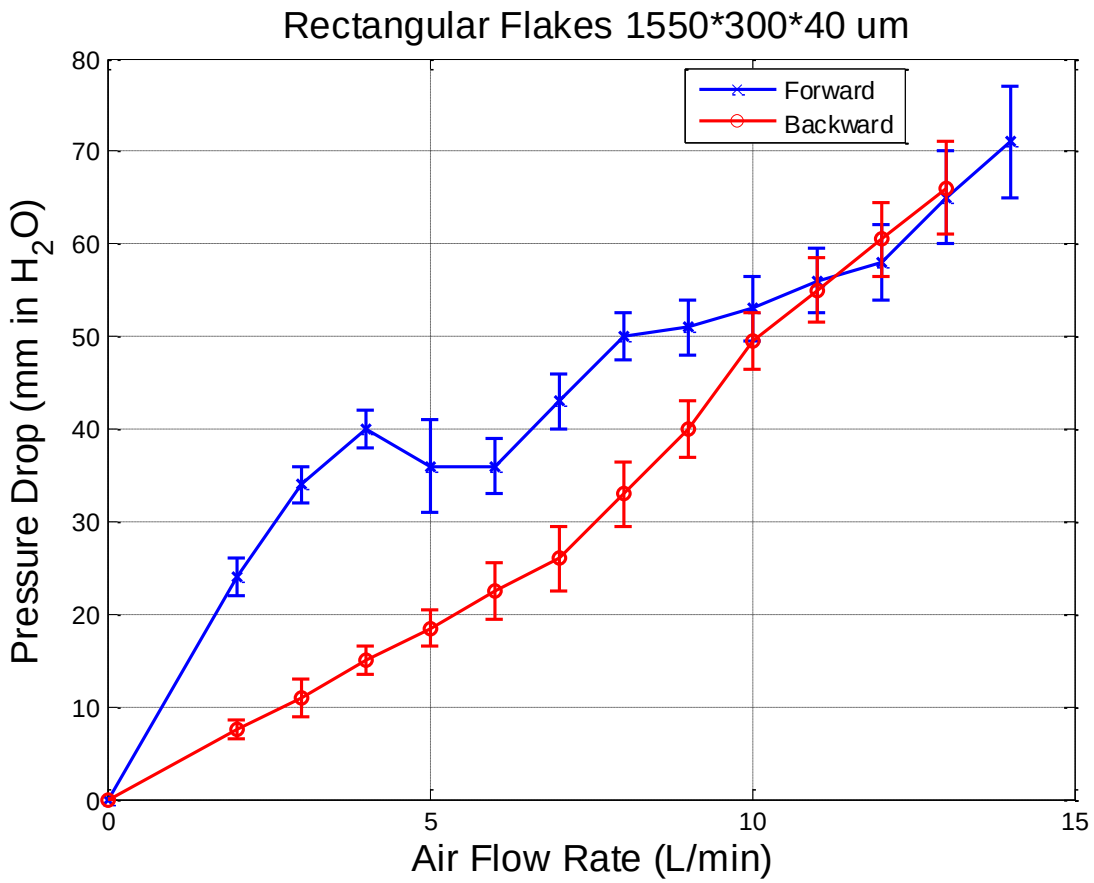

Figure A-5. Pressure drop versus air flow rate for plastic rectangular flakes 1550*300*40 μm.

LIST OF REFERENCES

[1] H.-. Xie, D. Geldart, Fluidization of FCC powders in the bubble-free regime: effect of types of gases and temperature, Powder Technol 82 (1995) 269-277.

[2] W. Yang, Modification and re-interpretation of Geldart's classification of powders, Powder Technol 171 (2007) 69-74.

[3] R. Di Felice, L.G. Gibilaro, Wall effects for the pressure drop in fixed beds, Chemical Engineering Science 59 (2004) 3037-3040.

[4] B. Eisfeld, K. Schnitzlein, The influence of confining walls on the pressure drop in packed beds, Chemical Engineering Science 56 (2001) 4321-4329.

[5] R.P. Chhabra, Estimation of the minimum fluidization velocity for beds of spherical particles fluidized by power law liquids, Powder Technol 76 (1993) 225-228.

[6] C. Lin, M. Wey, S. You, The effect of particle size distribution on minimum fluidization velocity at high temperature, Powder Technol 126 (2002) 297-301.

[7] Martin Rhodes, Introduction to particle technology, 2nd ed., John Wiley & Sons, Ltd, Chichester, England, 2008.

[8] T. Li, S. Li, J. Zhao, P. Lu, L. Meng, Sphericities of non-spherical objects, Particuology 10 (2012) 97-104.

[9] C.Y. Wen, Y.H. Yu, A generalized method for predicting the minimum fluidization velocity, AIChE J. 12 (1966) 610-612.

[10] M. Hartman, O. Trnka, K. Svoboda, Fluidization characteristics of dolomite and calcined dolomite particles, Chemical Engineering Science 55 (2000) 6269-6274.

[11] H.J. Subramani, M.B. Mothivel Balaiyya, L.R. Miranda, Minimum fluidization velocity at elevated temperatures for Geldart’s group-B powders, Exp. Therm. Fluid Sci. 32 (2007) 166-173.

[12] R. Coltters, A.L. Rivas, Minimum fluidation velocity correlations in particulate systems, Powder Technol 147 (2004) 34-48.

[13] F. Benyahia, K.E. O'Neill, Enhanced Voidage Correlations for Packed Beds of Various Particle Shapes and Sizes, Particulate Science & Technology 23 (2005) 169-177.

[14] A. Delebarre, Revisiting the Wen and Yu Equations for Minimum Fluidization Velocity Prediction, Chem. Eng. Res. Design 82 (2004) 587-590.

[15] P. Bourgeois, P. Grenier, The ratio of terminal velocity to minimum fluidising velocity for spherical particles, The Canadian Journal of Chemical Engineering 46 (1968) 325-328.

[16] Anon, Velocity-voidage relations for sedimentation and fluidization, Chemical engineering science (1979) 1419-1422.

[17] D.C. Chitester, R.M. Kornosky, L. Fan, J.P. Danko, Characteristics of fluidization at high pressure, Chemical Engineering Science 39 (1984) 253-261.

[18] J. Reina, E. Velo, L. Puigjaner, Predicting the minimum fluidization velocity of polydisperse mixtures of scrap-wood particles, Powder Technol 111 (2000) 245-251.

[19] S.K. Gupta, V.K. Agarwal, S.N. Singh, V. Seshadri, D. Mills, J. Singh, C. Prakash, Prediction of minimum fluidization velocity for fine tailings materials, Powder Technol 196 (2009) 263-271.

[20] Z.L. Arsenijevic, Z.B. Grbavcic, R.V. Garic-Grulovic, F.K. Zdanski, Determination of non-spherical particle terminal velocity using particulate expansion data, Powder Technol 103 (1999) 265-273.

[21] A.W. Nienow, P.N. Rowe, L.Y.-. Cheung, A quantitative analysis of the mixing of two segregating powders of different density in a gas-fluidised bed, Powder Technol 20 (1978) 89-97.

[22] N.S. Grewal, S.C. Saxena, Comparison of commonly used correlations for minimum fluidization velocity of small solid particles, Powder Technol 26 (1980) 229-234.

[23] D.S. Povrenović, D.E. Had?ismajlović, ?.B. Grbav?i?, D.V. Vukovi?, H. Littman, Minimum fluid flowrate, pressure drop and stability of a conical spouted bed, The Canadian Journal of Chemical Engineering 70 (1992) 216-222.

[24] R. Solimene, A. Marzocchella, P. Salatino, Hydrodynamic interaction between a coarse gas-emitting particle and a gas fluidized bed of finer solids, Powder Technol 133 (2003) 79-90.

[25] B. Liu, X. Zhang, L. Wang, H. Hong, Fluidization of non-spherical particles: Sphericity, Zingg factor and other fluidization parameters, Particuology 6 (2008) 125-129.

[26] J. Reina, E. Velo, L. Puigjaner, Predicting the minimum fluidization velocity of polydisperse mixtures of scrap-wood particles, Powder Technol 111 (2000) 245-251.

[27] C.C. Xu, J. Zhu, Prediction of the Minimum Fluidization Velocity for Fine Particles of various Degrees of Cohesiveness, Chem. Eng. Commun. 196 (2009) 499-517.

[28] M. Leva, Fluidization, McGraw-Hill, New York, 1959.

[29] G.G.b.1. Brown, Unit operations, Wiley, New York, 1950.

BIOGRAPHICAL SKETCH

Lingzhi Liao was born and raised in Hunan, in the People's Republic of China. She attended Centre South University where she received a Bachelors in Chemical Engineering and Technology. After graduating, she continued her Masters studies at the University of Florida. At the University of Florida, Lingzhi has held the social chair position in the Graduate Association of Chemical Engineers (GRACE), and won the Graduate Student Council's award of Outstanding Organization of the year.